A comparison between late summer 2012 and 2013 water masses, macronutrients, and phytoplankton standing crops in the northern Bering and Chukchi Seas

Revised manuscript for DSR-II Special Issue on the Arctic Eis field program

Seth L. Danielson[1], Lisa Eisner[2], Carol Ladd[3], Calvin Mordy[3,4], Leandra Sousa[5], and Thomas J. Weingartner[1]

30 March 2016

Corresponding author: Seth Danielson, sldanielson@alaska.edu

[1] School of Fisheries and Ocean Science, Institute of Marine Science, University of Alaska Fairbanks, Fairbanks, AK, USA, 99775-7220

[2]Alaska Fisheries Science Center, NOAA, 7600 Sand Point Way, Seattle, WA, USA 98115

[3] Pacific Marine Environmental Laboratory, NOAA, 7600 Sand Point Way, Seattle, WA, USA 98115-6349

[4] Joint Institute for the Study of the Atmosphere and Ocean, University of Washington, Seattle, WA

[5] North Slope Borough Department of Wildlife Management, PO Box 69, Barrow, AK, USA 99723-0069

Keywords: Bering Sea, Chukchi Sea, nutrients, phytoplankton, water mass, wind, Alaskan Coastal Current, ice melt

Abstract

Survey data from the northern Bering and Chukchi sea continental shelves in August-September 2012 and 2013 reveal inter-annual differences in the spatial structure of water masses along with statistically significant differences in thermohaline properties, chemical properties, and phytoplankton communities. We provide a set of water mass definitions applicable to the northern Bering and Chukchi continental shelves, and we find that the near-bottom Bering-Chukchi Summer Water (BCSW) was more saline in 2012 and Alaskan Coastal Water (ACW) was warmer in 2013. Both of these water masses carried higher nutrient concentrations in 2012, supporting a larger chlorophyll *a* biomass that was comprised primarily of small (<10 μm) size class phytoplankton, so the classical relation between higher nutrient loads and larger phytoplankton does not hold for this region in late summer. The distributions of phytoplankton biomass and size structure reveal linkages between the wind fields, seafloor topography, water mass distributions and the pelagic production. The water mass structure, including the strength and location of stratification and fronts, respectively, differed primarily because of the August regional wind field, which was more energetic in 2012 but was more persistent in direction in 2013. High concentrations of ice in winter and early spring in 2012 and 2013 resembled conditions of the 1980s and early 1990s but the regional ice retreat rate has accelerated in the late 1990s and 2000s so the summer and fall ice concentrations more closely resembled those of the last two decades. Our data show that wind forcing can shut down the Alaskan Coastal Current in the NE Chukchi Sea for periods of weeks to months during the ice-covered winter and during the summer when buoyancy forcing is at its annual maximum. We hypothesize that a decrease in salinity and nutrients from 2012 to 2013 was a consequence of a decreased net Bering Strait transport from 2011 to 2012. Biological ramifications of an accelerated ice melt-back, restructuring of shelf flow pathways, and inter-annually varying Bering Strait nutrient fluxes are mostly unknown but all of these variations are potentially important to the Arctic ecosystem. Our results have implications for the total magnitude

and seasonal evolution of primary productivity, secondary production, and the fate of fresh water, heat, and pelagic production on the Bering-Chukchi shelves.

1. Introduction

The changing climate and diminishing sea ice impart a cascade of effects upon the sub-arctic and arctic marine ecosystem including species range alterations (e.g. Mueter and Litzow, 2008; Logerwell et al., 2015) and potentially increased access for human activities such as tourism, industrial development, and commercial fishing (Moran and Farrell, 2011; NRC, 2014). Consequently, periodic surveys to document the state of the ecosystem are required to maintain an up-to-date understanding and inform resource managers and policy makers. The Arctic Ecosystem Integrated Survey (Arctic Eis) program represents a multi-disciplinary approach to fulfilling such information needs through oceanography, plankton, fisheries, and seabird/marine mammal surveys coupled with a variety of discipline-specific process studies. In the context of the flow field, ice cover, and atmospheric conditions, this manuscript describes physical, chemical, and phytoplankton observations conducted as part of the August-September 2012 and 2013 Arctic Eis ship-based surveys. Our goal is a better understanding of how the currents, ice, and atmosphere affect this region's physical hydrography, macronutrients, and phytoplankton standing stock in August and September. Our observations and analyses provide a physical and chemical backdrop for the Arctic Eis study and other marine ecosystem studies conducted in the northern Bering and Chukchi seas in 2012-2013.

1.1. Oceanographic setting

The northern Bering and Chukchi Sea continental shelf waters and the regional marine ecosystem are all dominated by the influence of the northward-flowing Bering Strait flow field (Figure 1). This transport is driven by a seasonally fluctuating Pacific-Arctic pressure head

(Stigebrandt, 1984; Aagaard et al., 2006) that transmits ~ 1.0-1.2 Sv (1 Sv = 10^6 m^3 s^{-1}) during summer and ~0.5-0.6 Sv during winter months (Woodgate et al., 2005a). The flow field is strongly steered by the coastlines and the seafloor bathymetry on these two expansive (~ 800 km wide) continental shelves. Water flowing through Bering Strait is routed across the Chukchi shelf along three principal conduits: Herald Canyon in the west, Barrow Canyon in the east and the Central Channel across the mid-shelf, although wind driven and other fluctuations modify or at times even reverse these flows (Roach et al., 1995; Winsor and Chapman, 2004; Weingartner et al., 2005; Woodgate et al., 2005b; Spall, 2007).

Flow field fluctuations are driven directly by local wind stress (Aagaard et al., 1985), in addition to the remotely driven influences of propagating shelf waves and changing Ekman suction over the North Pacific sub-arctic gyre that alters the Pacific-Arctic pressure head (Danielson et al., 2014). The Bering Strait flow reverses with regularity during winter months, but rarely for more than a week or two at a time (Roach et al., 1995). Other non-steady currents are driven by baroclinic jets associated with the fresh coastal water (Gawarkiewicz et al., 1994; Weingartner et al., 1999), dense polynya water (Danielson et al., 2006) and marginal ice zone (MIZ) meltwater fronts (Lu et al., in revision), and the high frequency tidal and inertial motions. Tidal currents near St. Lawrence Island can exceed 20 cm s^{-1} (Danielson and Kowalik, 2005), but they are much weaker across the Chukchi Sea, where they exceed 5 cm s^{-1} only in Kotzebue Sound and near Wrangel Island (Danielson, 1996). In summer, the Alaskan Coastal Current (ACC) is a low-salinity and warm flow associated with coastal runoff and solar heating of the shallow and turbid nearshore zone (Coachman et al., 1975). All of these fluctuating currents are locally important to the region's biology via their roles in advecting nutrients, mixing subsurface nutrients into the euphotic zone, aggregating prey along convergent fronts, and dispersing passively drifting eggs and larvae.

The northern Bering Sea provides fresh water, nutrients, and organic matter to the Chukchi Sea through Bering Strait (Walsh et al., 1989). Waters from three distinct origins comprise this

flow: Anadyr Water (AW), Alaska Coastal Water (ACW), and Bering Shelf Water (BSW) (Coachman et al., 1975). Typically found along the Siberian coast and the western portion of Bering Strait, AW is relatively saline, cold, and nutrient-rich (Sambrotto et al., 1984). Limited observations (Overland et al., 1996), numerical modeling (Kinder et al., 1986; Overland and Roach, 1987; Clement et al., 2005; Danielson et al., 2012a), and the tracing of water mass characteristics (Coachman et al., 1975) identify the upper slope of the Bering Sea basin as the probable source for AW. The Anadyr Current circumscribes the Gulf of Anadyr in a clockwise fashion, carrying AW to Anadyr Strait, Chirikov Basin, Bering Strait, and thence to the Chukchi Sea. Along the Alaskan coast, relatively low-salinity water carries the markings of terrestrial discharge (Coachman et al., 1975; Iken et al., 2010) from the Yukon River, the Kuskokwim River, and other numerous smaller drainage basins. Bering shelf water is comprised of a mixture of slope and coastal waters.

The multi-month journey of Pacific-origin waters into the Arctic dictates that the seasonally varying influences of atmosphere-ocean heat fluxes significantly modify these waters en route. In the oceanic heat loss phase of the year (approximately October through April), much of the water on these shallow (< 50 m) shelves cools to and remains near the freezing point (e.g. Woodgate et al., 2005, a,b). Pacific Winter Water represents an important source for feeding the cold halocline of the Arctic Ocean (Aagaard and Carmack, 1981). The characteristic salinity signature of the AW, BSW and ACW may even be removed through the influence of brine-induced salinization in leads and polynyas in winter and through the influence of sea-ice melt and river discharges in summer. In the oceanic heat gain phase of the year the atmosphere is a net source of heat to the ocean and heat is carried into the Arctic by the Bering Strait throughflow. The location and timing of the various heat contributions determines whether it is available to melt ice, influence fall freeze-up, or is subducted into the interior (Shimada et al., 2006; Woodgate et al., 2010; Timmermans et al., 2014).

Critically important to the biology of the northern Bering and southern Chukchi seas is the delivery of high levels of nutrients (e.g., nitrate > 10 μM) to Chirikov Basin, a highly productive

126 region of the shelf (250–300 g C m^{-2} y^{-1}) (Sambrotto et al., 1984; Grebmeier et al., 1988; Springer,
127 1988; Walsh et al., 1989) that lies ~500 km from the nearest continental slope and deep-water
128 nutrient reservoir. Despite the shallow depths and large transit distance, the AW nutrient flux into
129 Chirikov Basin is maintained by the persistent Pacific-Arctic pressure head (Stigebrandt, 1984)
130 rather than the intermittently persistent wind-forced coastal upwelling that drives the majority of
131 the world's most productive shelf ecosystems (Mann and Lazier, 1991). Flow rates and nutrient
132 fluxes are particularly elevated throughout the long summer season when the Bering Strait
133 transport is at its annual maximum (Woodgate et al., 2005a), winds are weak and stratification is
134 strong so flow reversals in Bering Strait are infrequent (Coachman, 1993; Danielson et al., 2014).
135 Nearly 24 hours of sunlight are available to support primary production. As AW is first drawn
136 through the narrow Anadyr Strait and then the narrow Bering Strait, nutrients are presumably
137 delivered to the euphotic zone via mixing induced by the high levels of total kinetic energy, eddy
138 kinetic energy and bottom stress that characterize the current field here (Clement et al., 2005).
139 In contrast, low levels of surface nutrients, chlorophyll *a* (Chl*a*), and phytoplankton
140 productivity (~ 80 g C m^{-2} y^{-1}) are typically observed in ACW after the spring bloom and associated
141 nutrient depletion (Springer and McRoy, 1993). Farther north in stratified areas of the Chukchi Sea,
142 late summer and early fall surface nutrient depletion and a shallow pycnocline can lead to
143 formation of subsurface Chl*a* maxima with peak values more than an order of magnitude greater
144 than the near-surface concentrations (Cota, 1996; Cotispoti, 2005; Hill and Cota, 2005; Martini et
145 al., 2016). Furthermore, melting sea ice and snow pack through late spring and summer months
146 expose shelf waters to sufficient insolation to fuel new production, even in the presence of ice
147 cover, and both water column and sympagic production can commence prior to full ice retreat
148 (Arrigo et al., 2014). Phytoplankton community composition and phytoplankton biomass
149 concentrations also vary among water masses, with large chain-forming diatoms typically observed

150 within high Chl*a* regions and smaller taxa such as phytoflagellates observed in low nutrient waters
151 outside of the Anadyr plume region (Springer and McRoy, 1993).
152 Against this backdrop of elevated nutrient fluxes, uptake rates and productivity, the study
153 region as a whole is characterized by strong pelagic-benthic coupling resulting from water column
154 production, which often exceeds grazing capacity (Grebmeier et al., 1988) and in turn supports
155 benthic foraging of upper trophic level organisms including seabirds (Hunt and Harrison, 1990),
156 grey whales (Coyle et al., 2007) and walrus (Jay et al., 2012; 2014). Thriving epibenthic and infaunal
157 communities populate nearshore regions, influenced by ACW, such as Kotzebue Sound and Norton
158 Sound (Feder and Jewett, 1981; Feder et al., 2007) and farther offshore where BSW and AW
159 dominate (Feder et al., 2007; Grebmeier et al., 1988; Iken et al., 2010). There exists a series of
160 regional benthic "hotspots" where the deposition fields support benthic communities having
161 biomass that regularly exceeds 15 g m^{-2} (Grebmeier et al., 2015)
162 Because long-lived benthic organisms are conveniently observable integrators of shifting
163 environmental conditions and top-down feeding pressures, the hotspots represent valuable
164 monitoring sites for detecting the biological impacts of change over time over a range of Pacific
165 sector latitudes (Grebmeier et al., 2006a; Iken et al., 2010). Repeat sampling of these hotspots is the
166 foundation of the international Distributed Biological Observatory (DBO) monitoring program
167 (Grebmeier et al., 2010; Grebmeier et al., 2015). Within (or near to) the Arctic Eis survey grid, the
168 DBO program includes five monitoring regions: SW of St. Lawrence Island (DBO 1), Chirikov Basin
169 (DBO 2), the southern Chukchi Sea southwest of Point Hope (DBO 3), near the southern side of
170 Hanna Shoal (DBO 4) and Barrow Canyon (DBO 5). Consequently, studies that attempt to
171 understand benthic hotspot changes over time need also an understanding of the controls that
172 mediate nutrient availability, pelagic productivity, and other bottom-up drivers.
173 While numerous oceanographic observations have been collected in portions of this region
174 during the open-water season and some even in ice cover, the Arctic Eis survey is perhaps the first

175 set of comprehensive physics-to-fish surveys covering such a large expanse of the northern Bering-
176 Chukchi shelves (U.S. waters only) between Nunivak Island in the central Bering Sea and Barrow
177 Canyon in the NE Chukchi Sea with such a tightly and regularly spaced set of stations. The service
178 oceanography components of the program were designed to provide environmental context for the
179 upper trophic level surveys, but these data also offer an unusual opportunity to examine inter-
180 annual and spatial variations across the region. Our objective in this paper is to document and
181 account for the observed hydrographic and biological distributions by characterizing horizontal
182 and vertical variations of the thermohaline, macronutrient and Chl*a* distributions, their year-to-
183 year differences and their co-variability. We show that some of the notable features captured by our
184 measurements can be ascribed to the influences of ice melt, wind forcing, and oceanic circulation.
185
186 **2. Data and Methods**
187 2.1. CTD data and bottle samples
188 Arctic Eis oceanographic data were collected at stations spaced 28 or 55 km apart,
189 depending on location, over a survey grid that spanned the US northeastern Bering Sea and Chukchi
190 Sea shelves (157-170 °W, 60-72 °N, Figure 1). Sampling occurred from 7 August – 24 September in
191 both 2012 and 2013, with a similar order of station occupations in both years. Sampling began in
192 Bering Strait on 7 August, progressing northward toward the Chukchi shelf break along zonal
193 transects until 8 September 2012 and 6 September 2013. Sampling recommenced in Bering Strait
194 on 10 September in both years, whereupon the survey vessel worked its way southward to 60 °N
195 during the last two weeks of the cruise.
196 At the primary stations spaced every 55 km, conductivity-temperature-depth (CTD)
197 measurements were collected with a Sea-bird (SBE) 911 or SBE 25 CTD equipped with a Wetlabs
198 Wet-Star fluorometer to estimate in vivo Chl*a*. A SBE 49 or SBE 19+ CTD towed obliquely with a
199 bongo net for zooplankton sample collection was deployed to obtain hydrographic data at higher

200 spatial resolution (between primary stations) along longitudinal transects in the Chukchi Sea. At
201 the primary stations, water samples for nutrients and total Chl*a* were collected at ~10 m intervals
202 (2-6 depths) and size-fractionated Chla at two of these depths (10 m and 30 m) during the upcast
203 with 5-L Niskin bottles attached to the CTD.
204 Water samples for dissolved inorganic nutrients (phosphate, silicic acid, nitrate, nitrite and
205 ammonium) were filtered through 0.45 μm cellulose acetate filters, frozen at -80 °C on board ship,
206 and analyzed at a shore-based facility. Measurements were made using automated continuous flow
207 analysis with a segmented flow and colorimetric detection. Standardization and analysis
208 procedures specified by Gordon et al. (1994) were closely followed including calibration of labware,
209 preparation of primary and secondary standards, and corrections for blanks and refractive index.
210 Protocols of Gordon et al. (1994) were used for analysis of phosphate, silicic acid, nitrate and
211 nitrite. Ammonium was measured using an indophenol blue method modified from Mantoura and
212 Woodward (1983).
213 Chl*a* samples were filtered through Whatman GF/F filters (nominal pore size 0.7 μm) to
214 estimate total Chl*a*, and through polycarbonate filters (pore size 10 μm) to estimate large-size
215 fraction Chl*a*. Filters were stored frozen (-80°C) and analyzed within 6 months with a Turner
216 Designs (TD-700) bench top fluorometer following standard methods (Parsons et al., 1984). In vivo
217 fluorescence data (Wet Labs Wetstar), calibrated with discrete Chl*a* samples by fluorometer and
218 year were used to calculate water column integrated Chl*a*. The integrated >10 μm (large) size-
219 fractionated Chl*a* was similarly estimated by multiplying the total integrated Chl*a* from calibrated
220 in vivo fluorescence data by the mean large-size fraction ratio (>10 μm Chl*a* /total Chl*a*) from
221 discrete samples. The integrated <10 μm (small) size-fractionated Chl*a* was estimated by
222 subtraction of the large-size fraction from the total integrated Chl*a*. We used in vivo Chl*a* data for
223 our integrations as discrete determinations of Chl*a* did not provide sufficient vertical resolution for
224 accurate water column integrations.

225 Statistical comparisons were conducted to determine significant interannual differences in
226 surface and deep nutrients and integrated Chl*a* for each water mass classification. Surface nutrients
227 were evaluated by surface water mass, deep nutrients by deep water mass, and integrated Chl*a* by
228 each combination of surface and deep water mass found in our survey area. All data were natural
229 log transformed prior to statistical analysis using one-way ANOVAs in SYSTAT.
230
231 2.2. Ocean Currents
232 Ocean circulation observations in the NE Chukchi Sea in 2012 and 2013 included
233 measurements of surface currents via land-based high frequency radar (HFR) stations, surface
234 currents via satellite-tracked drifters, and subsurface currents via taut-wire oceanographic
235 moorings. We used a selection of these data to characterize the flow field in the northernmost
236 portion of the Arctic Eis survey.
237 CODAR, Inc. long-range (5 MHz) Seasonde HFR stations were deployed at Barrow,
238 Wainwright, and Pt. Lay. HFR data grids were processed on an hourly basis, but diurnal ionospheric
239 activity at this latitude resulted in reduced data coverage for a portion of each day. Because of this,
240 the HFR data were binned into daily averages. HFR processing for these data are described in
241 Weingartner et al. (2013). Data were collected from all three sites through August and September
242 2012. Equipment difficulties in 2013 resulted in a week of missing data from Barrow and delayed
243 Point Lay data collection until 28 August.
244 Pacific Gyre MicroStar satellite-tracked surface drifters were programmed to collect hourly
245 or half-hourly Global Position System (GPS) fixes. The MicroStars employ a cross-shaped sail
246 tethered 1 m below the surface. Data were screened for GPS quality and indications of missing
247 drogues, although none of the drifters incorporated a drogue sensor. Other deployments of
248 MicroStar drifters that did incorporate drogue sensors suggest that drogue loss can become a
249 problem after 2 or 3 months. For this paper we present data only from within the first month after

250 deployment and we assume that drogue loss during this time is minimal. Drifter data examined
251 herein include 36 drifter tracks in 2012 and 52 drifters in 2013.
252 A mooring was deployed at site BC2 (70.9 °N, 159.9 °W)(Figure 1) for both 2012 and 2013,
253 although the battery died prior to recovery in both years, truncating the record before the Arctic Eis
254 surveys. Nevertheless, the mooring data from the months leading up to the survey reveal aspects of
255 the flow field and its influence on preconditioning the shelf waters sampled during August and
256 September. The BC2 mooring provides a record of the flows up and down Barrow Canyon
257 (Weingartner et al., 2013b).
258
259 2.3. Meteorological data
260 A moored meteorological buoy was deployed seasonally offshore from Pt. Lay in both 2012
261 and 2013 near 166.1 °W, 70.0 °N. The Pt. Lay mooring was deployed on August 10th in 2012 and on
262 August 1st in 2013 and recorded into October in both years. Measurement parameters include air
263 temperature, water temperature, solar radiation, and atmospheric pressure. A second buoy, named
264 the Klondike buoy, was deployed near 165.3 °W, 70.9 °N and measured significant wave height and
265 direction from August 21 into October in both years. Hourly observations were transmitted in real
266 time to UAF and converted to engineering units using factory calibration coefficients.
267 Nominally hourly weather conditions (wind speed and direction, air temperature, relative
268 humidity, atmospheric pressure, sky cover) recorded at the Barrow airport were obtained from the
269 National Climate Data Center (http://www.ncdc.noaa.gov/). All data were error-checked for sensor
270 spikes, stuck readings and other obviously erroneous data. These data are part of the long-term
271 weather record at Barrow, which extends back to 1920 for temperature and sea level pressure and
272 back to 1936 for winds.
273
274 2.4. Passive microwave sea ice concentrations

Satellite-based sea ice concentration data from 1979-2014 were downloaded from the National Snow and Ice Data Center (NSIDC) archive of the Goddard Space Flight Center NASA team dataset (http://nsidc.org/data/docs/daac/nsidc0051_gsfc_seaice.gd.html). These data were collected on the Nimbus-7, DMSP-8, -F11, -F13, and -F17 satellites and reported on a nominally 25 km grid (Cavalieri et al., 1996). Data were collected after July 1987 on a daily basis, while data before this were collected every other day. We linearly interpolated the earlier records to daily intervals.

2.5. Streamflow

Quality-controlled river discharge records for 2012 and 2013 were obtained from the USGS on-line database for the Yukon River Pilot Station monitoring site located at 61°56'04"N, 162°52'50"W (http://waterdata.usgs.gov/nwis/inventory?agency_code=USGS&site_no=15565447). These data required no additional processing.

3. Results

Although the two surveys are not synoptic, the success of the Arctic Eis program in occupying the same stations with nearly identical day of year timing in the two field efforts provides a remarkably consistent dataset for inter-annual comparison. We are unable to differentiate some aspects of seasonality and spatial variability.

3.1. Sea Ice

The range of satellite-observed daily ice concentrations for two 17-year intervals, 1979-1996 and 1997-2014, along with the envelope that contains the overlap in range are shown in Figure 2a. This depiction ignores regional spatial heterogeneity (Frey et al., 2015) but emphasizes extreme

300 events that push the regional ranges to new daily highs and lows. May-November tends to contain
301 mostly ice concentration minima during 1997-2014 and mostly maxima during the earlier period
302 (1979-1996), revealing the tendency for earlier retreat and delayed onset in recent years (Stroeve et
303 al., 2011). The lack of ice between spring and fall during the latter period is highlighted.
304 Figure 2a also shows that although 2012 and 2013 each exhibited multiple instances of
305 daily record high ice concentration in winter, these anomalies did not persist into the following
306 summers. Presumably, the ability for the system to shift so rapidly reflects the loss of ice mass
307 through net ablation and thinning of the ice pack (Kwok and Rothrock, 2009). While daily ice
308 concentrations in February-May were generally higher than the 1979-2014 daily averages in both
309 2012 and 2013, both years displayed concentrations well below normal by the end of June. The
310 passive microwave satellites reported ice-free waters by mid-August in both years (Figure 2a). As a
311 caution to interpretation, the Arctic Eis survey vessel did encounter appreciable ice in the northern
312 portion of the study grid that kept the vessel from working at a number of planned stations. In 2013,
313 ice was found consistently at locations on the northern shelf that were more than about 200 km
314 from shore. In August 2012, ice was near Hanna Shoal, including a very large piece (tens of km^2 in
315 area) of thick ice that grounded atop of Hanna Shoal during the winter. The tendency for passive
316 microwave satellites to under-estimate ice cover in regions of sparse and wet ice (Polashenski et al.,
317 2012) thus mandates an appreciation of this platform's limitations and a nuanced interpretation of
318 its data.
319 Temporal trends in the seasonal transition lengths for the study region are shown in Figure
320 2b, with recent years showing a spring transition that occurs nearly 30 days more quickly and a fall
321 transition that occurs nearly 40 days more quickly. The trends in each case are significant at the
322 99% level ($p < 0.001$), with $r^2 = 0.30$ and 0.29 for spring and fall, respectively. The length of time to
323 transition from ice-covered to ice free conditions in the spring and then from ice-free to ice-covered
324 conditions in the fall is potentially important physically and biologically.

325

326 3.2. Atmospheric conditions

327 Average monthly sea level pressure patterns (Figure 3) reveal strongly contrasting wind
328 fields in the two field years, particularly in August. In August 2012, low pressure was observed over
329 the northwestern Chukchi Sea leading to southwesterly (winds from the southwest) flow over our
330 study area. By September 2012, a low was positioned over western Alaska and the southeastern
331 Bering Sea, leading to northeasterly winds over the Chukchi Sea. In 2013, zonally elongated low
332 pressure patterns were present over the Bering Sea (August) and Gulf of Alaska (September),
333 promoting more zonal easterly flow over the Chukchi. These broad directional patterns were also
334 observed at the surface in Barrow, manifesting as differences in wind direction steadiness. For
335 example, in August 2012, Barrow weather station PABR recorded 100 hourly observations (~4
336 days in total) of winds blowing into the SW sector between 180 °T and 270 °T (°T denotes
337 directional orientation with respect to true North, where 0 °T is due North and 90 °T is due East),
338 whereas in August 2013 the winds blew into this sector for 383 hours (more than half of the
339 month). PABR recorded 306 hourly observations of winds blowing into the SW sector in September
340 2012 while September 2013 recorded 377 observations.

341 In addition to differences in wind direction, the August 2012 mean wind speed (WS)
342 recorded at Barrow was 1 m s^{-1} higher and with larger standard deviation (σ) than August 2013
343 (WS_{AUG12} = 5.52 m s^{-1}, σ_{AUG12} = 2.55 m s^{-1}; WS_{AUG13} = = 4.56 m s^{-1}, σ_{AUG13} = 1.99 m s^{-1}), reflected in
344 longer durations of strong winds (2012 recorded 379 hourly observations of wind speed >= 5 m s^{-1},
345 while August 2013 recorded only 223). Like the wind directions, September 2012 and September
346 2013 wind speeds were quite similar to each other (WS_{SEP12} = 5.23 m s^{-1}, σ_{SEP12} = 2.54 m s^{-1}; WS_{SEP13}
347 = 5.56 m s^{-1}, σ_{SEP13} = 2.58 m s^{-1}).

348 The Pt. Lay surface meteorological buoy shows that August 2013 winds were directed more
349 to the west and south, carrying cool air temperatures above warmer sea surface temperatures

(Figure 4). There was more incident solar radiation in August 2013 (fewer clouds), while 2012 had deeper dips in the recorded atmospheric pressure record. Despite these differences in solar radiation, water temperatures in September 2013 were slightly cooler. Over the August 21 to September 30 interval, the Klondike mooring recorded more large (> 3 m) swells in 2012, which were present for about 15% more of the time in this year. In accordance with the inter-annual differences in wind direction observed by the mooring and at station PABR, the dominant wave direction in 2013 favored wave propagation from the ENE octant, whereas the waves in 2012 were more evenly distributed from the NNW, NNE and ENE octants.

3.3. Currents

The pronounced differences observed in the wind field were reflected in the oceanic response of near-surface currents as measured by surface 1-m drogued drifters and the HFR, despite spatial and temporal data gaps that hinder interpretation of both sets of measurements.

On average, surface velocities in August 2012 as measured by the HFR (Figure 5) exhibited a strong ACC in the vicinity of Barrow Canyon with northeastward flow over the entire region. There was particularly strong eastward flow in the region bounded by the coast, 162 °W, and 71.5 °N. In September 2012, when northeasterly winds prevailed the mean flow reversed to the southwest, but was generally weak. The mean August 2013 HFR record (biased by missing data) indicated a weak ACC flowing to the northeast and northwestward flow over Hanna Shoal. September 2013 winds reversed the flow along the coast and waters over the shelf offshore of Barrow Canyon flowed toward the northwest. We also note that Northeastward transport calculated from moorings deployed off of Icy Cape was much weaker than average during August 2013 while August 2012 transport was closer to a 5-year climatology (Stabeno, et al., accepted).

In 2012, drifters deployed offshore near 70.5 °N, 164 °W progressed toward the Alaskan coast between 11 August and 30 August (Figure 6). Drifters deployed < 15 km from shore were

375 caught in the coastal flow and accelerated eastward into Barrow Canyon. On August 30 and 31,
376 upwelling-favorable winds reversed the shelf flow and many drifters moved westward for about a
377 week, after which the currents reverted to their initial direction and drifters close to Barrow
378 Canyon were swept into the ACC. Upon reaching the slope region, drifters that moved down Barrow
379 Canyon either turned to the northwest, turned east onto the Beaufort Sea shelf, or moved off the
380 shelf and into the basin. In contrast, the 2013 drifters primarily headed to the west and the south
381 and none of the 2013 drifters left the shelf via Barrow Canyon in August or September. Many of the
382 2013 drifters wound up beaching on the Chukchi's Siberian coastline.
383 Currents earlier in the year preceding the Arctic Eis cruises also exhibited contrasting flow
384 regimes that likely influenced the winter and spring hydrographic conditions at least on the NE
385 Chukchi shelf. Mooring BC2, located near the head of Barrow Canyon, recorded essentially no net
386 flow along the axis of the canyon for the 4-month interval January-April 2012 (not shown). In
387 contrast, from the last week of December 2012 through mid-March 2013 the flow was nearly
388 continuously *up-canyon* (along ~ 243 °T, directed from the basin to the shelf). Associated with this
389 flow reversal was, at times, an extensive coastal polynya that was captured by the passive
390 microwave satellite observations as an ice concentration minimum and that extended from Point
391 Barrow southward past Point Hope and over 100 km offshore. In both years, flow between the start
392 of May and mid-July was primarily down-canyon, i.e., toward the basin.
393
394 3.4. Physical hydrography
395 3.4.1. Water Mass Identification
396 Examining all 1-m averaged T/S measurements from the two cruises, we subjectively
397 parsed the data into five bounding boxes (Figure 7 and Table 1) that encompass all observed water
398 types, including eight distinct water masses: Alaskan Coastal Water (ACW), Anadyr Water (AW),
399 Bering Sea Summer Water (BSSW), Bering Sea Winter Water (BSWW), Chukchi Sea Summer Water

(CSSW), Chukchi Sea Winter Water (CSWW), and Atlantic Water (AtlW). On the Bering shelf, BSWW is commonly referred to as "cold pool" water (e.g., Takenouti and Ohtani, 1974), although an upper temperature bound for cold pool water is often taken at 2 °C (e.g., Stabeno et al., 2002). For the purposes of this study, we often refer to aggregate water masses that encompass the AW/BSSW/CSSW and BSWW/CSWW water types as Bering-Chukchi Summer Water (BCSW) and Bering-Chukchi Winter Water (BCWW), respectively.

In some instances we do need to distinguish between the constituent water masses that comprise the BCSW and BCWW aggregates because of different locations, time histories, and the different roles that they play in the ecosystem. For example, BSWW and CSWW are both cold remnants of the previous winter's heat loss but at summer's end they lie hundreds of kilometers to either side of Bering Strait. Similarly, AW, BSSW and CSSW are indistinguishable here based on their T/S properties alone. AW is generally known as the saline nutrient-rich water delivered across the Gulf of Anadyr to Bering Strait (Coachman et al., 1975). BSSW and CSSW can achieve the same T/S properties as AW through the cycles of freezing, brine rejection, and then summer warming, but they lack the important slope-derived AW nutrient load.

For water masses named by one end member only (e.g., MW and AtlW), we caution that interpretation of habitat or other features based on the names alone can be misleading. For example, the influence of Atlantic Water (AtlW) is identified by the tightly clustered line of points that trends away from the near-freezing winter water for salinities greater than about 33.5. Of course, all points lying along such a mixing line would have contributions from both the CSWW and AtlW end members, but the relative fractions vary inversely with distance along the mixing line and water with salinity closer to 33.5 are comprised of more CSWW than AtlW.

3.4.2 Water mass distributions

Because the two cruises occupied most stations on nearly the same year-day, inter-annual differences in water mass extents reflect year-to-year differences in the forcing and/or circulation. Distributions of the water masses in each year are mapped in Figure 8. Figure 9 shows maps of averaged near-surface (0-10 m) and near-bottom (within 5 m of each CTD cast's deepest depth) temperatures and salinities. Figure 10 includes maps of surface-to-bottom density differences to show the average water column stratification and the magnitude of the horizontal density gradient to show the location of near-surface and near-seafloor fronts.

The one station having AtlW was located at the mouth of Barrow Canyon at an upper slope station that was occupied in 2013 but not in 2012. The maximum CTD depth recorded in 2012 was 88 m (with a bottom depth of 99 m), while in 2013 the CTD reached 274 m at the station with AtlW (bottom depth of 289 m).

ACW was observed close to shore from Nunivak Island to Point Barrow in 2012 but in 2013 only as far north as Ledyard Bay. These data support the drifter and HFR suggestions (Section 3.2) of an ACC that was mostly absent from the NE Chukchi Sea during the 2013 cruise. It appears that the ACW was able to round Cape Lisburne but not progress appreciably farther along the coast in 2013. Examination of true color satellite imagery (not shown) suggests that Ledyard Bay is often the site of a recirculation cell where a portion of the ACC flow stalls, while the Point Hope and Cape Lisburne promontories and associated bathymetry commonly deflect some of the ACC offshore. Farther south in the Bering Sea, ACW spread at least 100 km farther offshore from the Yukon-Kuskokwim Delta in 2013, occupying most of the surface mixed-layer. Together these observations show strongly contrasting ACW behaviors and pathways during the two Arctic Eis surveys in both the southern and northern portions of the survey.

The BCSW range of properties were found at most stations, with exceptions at some coastal stations having only ACW and at some stations occupied instead by only MW and WW in the very northernmost portion of the survey grid. Although ACW was absent from the northwest Alaskan

449 coast in 2013, CSSW was located at half a dozen stations adjacent to the coast between Point Lay
450 and Barrow. Along with the greater penetration of ACW into the northern Chukchi Sea in 2012, the
451 northern edge of the CSSW was farther north in 2012 than in 2013. Even in 2012, however,
452 relatively few stations with CSSW were found near Hanna Shoal, a known area of flow stagnation
453 (Martin and Drucker, 1997). Instead, particularly in 2013, we observed MW overlying CSWW near
454 Hanna Shoal. Between St. Lawrence and Nunivak Islands, the presence of ACW and BSWW in layers
455 of at least 10 m thick each (Figure 8) mostly displaced or precluded any BSSW here in 2013, which
456 occupied only a 1-3 m thick layer at eight stations (and could have been the result of mixing
457 between the upper and lower layers). Comparison of the BCSW properties (Figure 7 and Table 2)
458 shows that the 2013 salinities in the northern Chukchi Sea were appreciably lower than in 2012
459 (despite the large and long-lived 2013 mid-winter polynya). The primary mixing line about which
460 most data points are clustered (through the BCSW box in Figure 7 that runs between the ACW and
461 BCWW boxes) shows a salinity offset of about -0.5 in the 2013 data.
462 MW was confined solely to the northern and northeastern Chukchi shelf. In 2012 it was
463 located mostly offshore, while in 2013 it extended all the way to the NW Alaskan coast, occupying
464 stations at which we might have expected ACW instead. The vessel did not sample the farthest
465 northwest corner of the planned survey grid in 2013 but based on the maps shown in Figure 8, we
466 may infer that CTDs at these missed stations would have found MW and CSWW, and possibly a
467 contribution from CSSW. The theta-S diagrams shown in Figure 7 show a much larger number of
468 MW observations in 2013 relative to 2012. Along with ACW in Norton Sound, MW over Hanna Shoal
469 contributed to the strongest levels of vertical stratification observed in the survey (Figure 10).
470 CSWW was confined to the northeast Chukchi Sea but with a somewhat greater lateral
471 extent (50-150 km) to the south and west than the MW. In the Bering Sea, we found BSWW at seven
472 stations south of St. Lawrence Island in 2013 and at one station in Chirikov Basin in 2012. Along
473 with the 2012/2013 differences in salinities and currents noted above, these data also suggest that

474 the northern Bering and Chukchi shelf of 2013 may have experienced less (or different) flushing
475 between winter's end and the cruise than during the same time period in the prior year. A striking
476 example is seen in Figure 7 between the sigma-theta 26 and 27 isopycnals, in which we see
477 considerably denser water on the northern Chukchi shelf in 2012. This stands in contrast to the
478 extended upcanyon flow observed at mooring BC2 in the middle of the 2013 winter, from which we
479 might have expected that the low ice concentrations would have promoted greater polynya activity
480 and shelf densification. We do observe more CSWW data points within the 2013 BCWW box, but the
481 salinity is lower on average.
482 At a number of stations north of 70 °N we found MW, CSWW and CSSW all present in the
483 same water column in both years. MW is always the least dense water mass of the three and CSWW
484 typically underlies CSSW. These intrapycnocline occurrences of BCSW between the other two water
485 masses may be the result of subducting CSSW as described by Lu et al. (2015).
486
487 3.4.3 Descriptive physical hydrography
488 In the northern Bering Sea south of St. Lawrence Island and in Norton Sound, surface waters
489 were warmer (by ~2 °C) and near-bottom salinities were fresher (by ~ 0.5) in 2013 than in 2012
490 (Figure 9). Near bottom temperatures in 2013 were warmer inside the ACW front and cooler
491 offshore, including the seven stations at which BSWW was observed. Although the station spacing
492 did not well resolve the frontal structure, year-to-year differences in the horizontal density
493 gradients suggest differences in the location and strength of the ACC jet (Fig 10). South of St.
494 Lawrence Island we find primarily ACW characteristics lying above BSWW (Figure 8); the front
495 near the seafloor primarily separates these two water masses without BSSW between.
496 Vertical stratification was weak in both years in Chirikov basin, just north (downstream) of
497 Anadyr Strait (Figure 10). Chirikov Basin was somewhat fresher during the 2013 survey both at the
498 surface and at depth, although temperatures were similar to those of 2012 (Figure 9). This area is

499 strongly influenced by the Anadyr Water flowing past the western side of St. Lawrence Island and
500 multiple processes may have contributed to the observed differences (e.g., water pathways, degree
501 of topographic or wind-induced mixing, flow rates and bottom friction). The lower salinities in
502 2013 are consistent with an offshore transport of coastal water that would conform to the winds
503 associated with the sea level pressure patterns shown in Figure 3.

504 Coastal water was appreciably warmer in 2013 between Nunivak Island and Ledyard Bay
505 (Figure 9). However, salinities just north of Bering Strait were much fresher in 2012 than in 2013
506 both near the surface and near the bottom except for at the stations along the US-Russia Convention
507 Line. These data suggest that the Yukon discharge was mostly trapped in Norton Sound or was
508 spread to the west and south in 2013, while the runoff was able to leak out of Norton Sound and
509 along the eastern shore of Bering Strait into the Chukchi Sea in 2012.

510 Water in Norton Sound were very fresh ($19 < S < 30$) in both years even below the surface
511 mixed-layer, reflecting the local influence of the massive freshwater input from the Yukon River (~
512 200 $km^3\ yr^{-1}$ on average (Aagaard et al., 2006)) and the long local residence time suggested by a
513 very few oceanographic drifters deployed in coastal water on the Bering shelf (T. Weingartner,
514 pers. comm.; also see www.ims.uaf.edu/drifters/). Peak Yukon River discharge measured at Pilot
515 Station occurs in June, and then slowly tapers off through October. Using recent and historical USGS
516 streamflow data from Pilot Station, we found that June 2013 exhibited one of the highest discharges
517 on record for this month, 20,100 $m^3\ s^{-1}$, 25% higher than the mean climatology of 16,200 $m^3\ s^{-1}$ (σ =
518 3,240 $m^3\ s^{-1}$). The 2012 discharge (17,700 $m^3\ s^{-1}$) was also higher than the June climatology but
519 within one standard deviation of the mean. Both the 2012 and 2013 total discharges were within
520 one standard deviation of the climatological discharge for July – August.

521 The warm and fresh signature of the ACW typically follows the Alaskan coast from Norton
522 Sound to Bering Strait and north toward Barrow Canyon, but as shown above in sections 3.2 and
523 3.3 a portion of the ACC appeared to shut down in 2013. The temperature and salinity distributions

524 clearly show this (Figure 9) as do the surface and bottom front locations (Figure 10). The CSWW
525 and MW near to the northwestern Alaskan coast in 2013 is consistent with coastal upwelling of
526 subsurface water due to offshore Ekman transport and/or upwelling of cold water from deeper in
527 Barrow Canyon.
528 Relative to 2013, saltier water was found near to the seafloor across much of the 2012
529 survey (Figure 9 and Table 2). A widespread change of salinity could be due to greater fraction of
530 AW occupying Chirikov Basin, greater ice production and shelf water salinization during the
531 previous winter, a reduced influence of melt water mixed over the water column, less lateral
532 exchange with fresh coastal water, or a combination of these processes. To the extent that higher
533 salinity water carries higher dissolved nutrient loads, there exists potential for these two years to
534 support contrasting levels of net biological production if the source of the salinity anomalies are
535 primarily tied to differences in the AW contribution to the shelf waters.
536
537 3.5. Nutrient hydrography
538 Macronutrient distributions exhibited year-to-year differences in both the surface (Figure
539 11 and Table 2) and near-bottom (Figure 12 and Table 2) layers. Despite a few similarities, the
540 nutrient fields, particularly for surface waters, did not closely resemble each other between 2012
541 and 2013, and many of the differences align with the different water mass distributions described
542 above (Figs. 9 -12; Tables 2 and 3). In 2012, surface nitrate potentially at or above limiting levels for
543 phytoplankton growth (> 1 μM) was observed from Chirikov Basin north to 67.5 °N. In contrast,
544 surface nitrate was very low (<= 1 μM) in 2013 at all but four stations in Chirikov Basin at 64-64.5
545 °N and one station at the head of Barrow Canyon at 70.5 °N; both areas also had high ammonium,
546 silicic acid and phosphate. Ammonium is a reduced and preferential nitrogen source for
547 phytoplankton growth (Dortch, 1990), and in 2012, near-surface ammonium concentrations > 1 μM
548 were common from just south of Bering Strait to the northernmost stations in the Chukchi Sea,

549 compared to 2013 when surface ammonium was very low (<= 1) at all but two stations. Surface
550 silicic acid was generally higher inshore than offshore in both years. The highest values (> 20 μM)
551 were observed in Norton Sound in both years and in Chirikov Basin in 2012, the year in which
552 salinity data indicated that the Norton Sound ACW low-salinity water flowed unimpeded northward
553 into the Chukchi Sea. Surface phosphate was generally lower in the Chukchi Sea and higher in the
554 northern Bering Sea in both years, although the highest values (> 0.75 μM) were observed in the
555 Chirikov basin at one station in 2013 and up to 67.5 °N in 2012 (at the same stations with high
556 nitrate). Surface phosphate was generally higher in 2012 compared to 2013, with the greatest
557 intrannual differences observed in Chirikov Basin and the Chukchi Sea.
558 In 2012 and 2013, at near bottom depths, higher nitrate, ammonium and phosphate levels
559 were observed in the colder, higher salinity BCWW and BCSW water masses, relative to the
560 generally (but not exclusively) nitrate-depleted shallower ACW stations located near the coast
561 (Figs. 8, 12, Table 2). Note that the high nutrient concentrations seen near shore at and north of 71
562 °N in 2013 were associated with BCWW and BCSW, since ACW did not reach that far north that
563 year. The geographic regions with highest near-bottom nutrients included Chirikov Basin, Bering
564 Strait (in both 2012 and 2013), southwest of Point Hope (in 2013) and two stations over Hanna
565 Shoal and the head of Bering Canyon, although values were lower in 2013 than in 2012, particularly
566 over Chirikov Basin and Bering Strait. Similar to surface water, near-bottom silicic acid was also
567 elevated at stations in Norton Sound. South of St. Lawrence Island near-bottom nutrient levels were
568 lower than those observed in Chirkiov Basin, presumably due to differences in total advective
569 inputs, drawdown rates, and/or the diluting effect of westward-progressing low-nutrient ACW that
570 emanates from the near-shore zone.
571 For the 38 Chukchi Sea stations sampled in both years, no systematic difference was found
572 in the integrated nitrate concentrations but relative to 2013, 2012 had significantly more water
573 column ammonium, phosphate, and silicate (significant at the 99%, 90%, and 99% levels,

574 respectively) (Tables 2 and 3; Figure 13). This result is consistent with the 2012 higher salinities
575 described above in Section 3.4. Nutrient limitation of phytoplankton growth in near-surface water
576 may have been considerably more widespread in 2013 than in 2012 because more stations had
577 non-limiting levels of nitrate, ammonium and silicic acid in 2012 (Figure 11).
578 Interannual comparisons indicate that nutrient concentrations also varied significantly
579 between years within water mass classifications. Surface ammonium and phosphate were
580 significantly higher in 2012 for all three surface water mass classifications MW, BCSW, ACW (Table
581 2). In addition, silicic acid was higher in MW and BCSW, and nitrate was higher in MW. Bottom
582 nutrients and bottom salinity were significantly higher in 2012 than in 2013 in the BCSW (Table 2),
583 due to differing inputs of the constituent water masses (AW, BSSW, CSSW). There were also more
584 stations having BCSW near the seafloor in 2012 than in 2013 (Figure 7). Bottom ammonium was
585 significantly higher in ACW in 2012 (Table 2). In the next section, we will show that these variations
586 in the nutrient loads were also associated with detectable changes in the phytoplankton.
587
588 3.6. Chlorophyll *a*
589 In 2012, near-surface Chl*a* from discrete samples (Figure 14) was highest (5-14 mg m^{-3}) at
590 Chirikov Basin stations with high nitrate and silicate concentrations (Figure 11). Figure 14 also
591 shows moderate (1-2 mg m^{-3}) 2012 Chl*a* levels across most of the northern Bering Sea, in a plume
592 emanating northward toward Point Hope from Bering Strait, and at coastal stations located
593 northeast of Cape Lisburne. In 2013, similar to 2012, discrete Chl*a* samples near the surface were
594 elevated in the DBO-3 region (Figure 14). Filtered seawater for Chl*a* was not available south of
595 Bering Strait in this year, however Chl*a* from calibrated in vivo fluorescence measurements (data
596 not shown) indicated high surface Chl*a* in Chirikov Basin at stations with relatively high surface
597 nutrient concentrations and high levels of integrated Chl*a*. Subsurface chlorophyll maxima in both
598 years were observed at ~ 20-30 m depths. In 2012, relatively high (1 m averages of 2-12 mg m^{-3})

599 subsurface Chl*a* was seen at some offshore locations near Point Hope, between 70 °N and 72 °N
600 over Hanna Shoal, and at two stations along 71°N (data not shown). Likewise, in 2013 subsurface
601 chlorophyll maxima were observed over Hanna Shoal (data not shown) in locations with integrated
602 Chl*a* of 26-50 mg m^{-2}.

603 Areas of high integrated Chl*a* (> 100 mg m^{-2}) included Chirikov Basin and, Bering Strait (in
604 both 2012 and 2013), and southwest of Point Hope (in 2013) and two stations over Hanna Shoal (in
605 2012)(Figure 15). Relatively high integrated Chl*a* (50-100 mg m^{-2}) was found at several other
606 stations in Chirikov Basin and Hope Basin. Chirikov Basin and SW of Point Hope encompass DBO
607 transects with a documented history of high primary production, phytoplankton standing crop, and
608 benthic biomass (Grebmeier et al., 2015). Integrated Chl*a* concentrations were moderate (26-50 mg
609 m^{-2}) over most of the survey region in 2012, and northwest of Nunivak Island in the south and over
610 Hanna shoal in the north in 2013. In general, Chl*a* biomass exhibited greater patchiness in 2013
611 with more observations at the low end of the range (Figure 15). For stations occupied in both years,
612 the average integrated Chl*a* was significantly lower in 2013 than in 2012 ($p < 0.05$) (Figure 15). In
613 particular, there was significantly lower integrated Chl*a* in 2013 at stations with ACW throughout
614 the water column or at stations with ACW overlying BCSW (Table 3). For both years combined,
615 there was significantly more integrated Chl*a* at stations having the BCSW bottom water mass than
616 ACW or CSWW ($p = 0.020$).

617 Small phytoplankton made up the majority of the Chl*a* biomass in the Chukchi Sea in 2012,
618 comprising at least 70% of the biomass at two-thirds (43/61) of the stations. In contrast, in 2013
619 fewer than half (24/54) of the stations had more than 70% small phytoplankton. Integrated large
620 size fraction Chl*a* (large phytoplankton) concentrations were very low (< 10 mg m^{-3}) at most
621 stations north of 69 °N in 2012, whereas low to moderate values (11-25 mg m^{-3}) were seen near
622 Hanna Shoal in 2013; note that in 2013 Chl*a* concentrations from large and small size fractions
623 were similar. While BCSW covered much more of the NE Chukchi shelf in 2012, 2013 was a year

624 with more extensive pools of MW and nutrient-rich CSWW. The percent large size phytoplankton
625 (>10 μm/total Chl*a*) were highest (> 50% large) offshore of Kotzebue Sound (DBO3 region) in both
626 years, suggesting that large taxa, such as diatoms or dinoflagellates, may make up a greater portion
627 of the total Chl*a* at this location, and particularly in 2013.
628 In contrast to a Chukchi shelf system dominated by small phytoplankton, large
629 phytoplankton dominated at about half of the Bering Sea stations (particularly near Nunivak
630 Island) in 2012, even though the Bering Sea stations were occupied after those in the Chukchi Sea.
631 Low to moderate Chl*a* concentrations were found in both large and small fractions at most Bering
632 Sea nearshore (ACW) stations.
633
634 **4. Discussion**
635 The character of the currents, air-sea interactions, and water properties on the Chukchi
636 shelf depends on wind velocity and wind persistence (e.g., Weingartner et al., 2005; Woodgate et al.,
637 2005b). While August 2012 had stronger winds than August 2013, the latter were more
638 directionally polarized, with nearly half the month experiencing wind that blew toward the south
639 and southwest. In response, ACW was not found north of Ledyard Bay in the 2013 Arctic Eis survey.
640 The 2013 winds forced surface water and satellite-tracked drifters westward and likely promoted a
641 several week period of upwelling in Barrow Canyon. Similarly, but for a much more prolonged
642 duration, we observed a multi-month Barrow Canyon flow reversal in early 2012 that likely
643 resulted in basin-shelf exchanges and heat loss to the atmosphere from the coastal polynya (Hirano
644 et al., 2016).
645 The ramifications of temporarily redirecting the more typical coastal flow pathway for
646 multiple weeks or months at a time are not clear, but there exists potential for both physical and
647 biological consequences (see, for example, papers in this volume by Marsh et al., Pinchuk and
648 Eisner, and Sigler et al.). Deposition of shelf-origin organic matter feeds benthic hotspots near

649 Hanna Shoal and Barrow Canyon, and reorganization of the shelf flow also suggests that a different,
650 and quite possibly lesser flux of carbon would have been deposited. However, one region's loss may
651 be another region's gain. If the Bering Strait throughflow is uncoupled from winds that locally
652 reverse the Barrow Canyon flow (an assumption that likely fails at least on occasion) then it would
653 appear that a greater fraction of the Bering Strait throughflow was probably directed
654 northwestward along the Siberian Shelf toward Herald Canyon and possibly Long Strait in 2013
655 (e.g., Luchin and Panteleev, 2014).
656 Taking the nutrient and chlorophyll observations of Sections 3.5 and 3.6 together, our
657 interpretation is that year-to-year differences in the location, magnitude and composition of the
658 phytoplankton community can be partially attributed to water mass distributions and their
659 associated nutrient loads. However, the classical assumptions that larger phytoplankton would be
660 associated with higher nutrient levels and higher biomass do not hold in these two years. The
661 higher nutrient concentrations and larger number of stations with bottom water mass BCSW could
662 both have contributed to the overall higher Chl*a* biomass in 2012. Not all differences were
663 associated with the BCSW, however. The more extensive spatial range of low levels of integrated
664 Chl*a* in nearshore water in 2013 were associated with reduced nutrient (ammonium and
665 phosphate) concentrations in ACW in this year (Tables 2 and 3). Higher ammonium concentration
666 in 2012 than in 2013 in all surface water masses, in ACW and BCSW bottom water suggest more
667 nutrient regeneration and regenerated production in 2012. The dominance of smaller
668 phytoplankton in 2012 also suggests the possibility of a more important microbial loop in this year.
669 It appears likely that all of these observed differences propagated farther up the food chain:
670 Pinchuk and Eisner (this volume) show differences that extend to the zooplankton as well.
671 The location of phytoplankton concentrations and their size compositions reveal some
672 consistent linkages between the wind fields, seafloor topography, water masses, and pelagic
673 production. The higher concentrations of large phytoplankton near Hanna shoal in 2013 suggest

674 that spatial variations in phytoplankton community composition between years were related to the
675 different lateral extent of the CSWW and MW distributions. A subsurface Chl*a* maximum was
676 detected over Hanna shoal and southwest of Point Hope in both years (compare Figs. 14 and 15,
677 Martini et al., 2016), whereas the bloom in Chirikov Basin was near the surface; surface nutrients
678 were available in the weakly stratified Chirikov Basin but not elsewhere. It is possible that the
679 Bering Sea phytoplankton were part of a fall bloom driven by the September low-pressure systems
680 and associated winds (Figs. 3 and 4), taking advantage of new nutrients introduced from below the
681 mixed-layer depth.
682 The annual average volume flux through Bering Strait exhibited an increase in northward
683 transport of ~ 50% from 2001 (0.7 Sv) to 2013 (1.1 Sv) (Woodgate et al., 2015; Woodgate et al.,
684 2012), and this increase corresponds to changes in heat and freshwater fluxes through the strait
685 and implications for nutrient fluxes (Woodgate et al., 2012). Annual mean transports through
686 Bering Strait during our two study years, 2012 and 2013, were at opposite extremes of the range
687 with very low (~0.7 Sv) and then high (~1.1 Sv) transport, respectively (Woodgate et al., 2015).
688 Another high transport year was 2011, with an estimated flux nearly the same as that in 2013
689 (Woodgate et al., 2015). We assume that a stronger Bering Strait flow represents a higher nutrient
690 flux and that water on the Chukchi shelf has a correspondingly smaller residence time. Although the
691 2012 to 2013 decrease in nutrients does not appear consistent with an increase in flow between
692 these two years, the decrease in flow from 2011 to 2012 could be consistent if the near-bottom
693 nutrients at the end of summer on the Chukchi shelf are a function of the previous year's Bering
694 Strait transport. The range of annual average transports through Bering Strait appears to match
695 the total shelf volume reasonably well for the ability of inter-annual flow variations to appreciably
696 impact nutrient concentrations over time scales of half a year to a year. For the southernmost
697 400,000 km^2 of the Chukchi shelf (the region south of about 72 °N), the entire volume could be
698 replaced in 6 to 10 months for average transports of 0.7 to 1.1 Sv. The annual (January-December)

699 integration period is likely not the proper time frame for consideration, but we expect that a more
700 detailed analysis of the Bering Strait mooring data would be no more conclusive given the small
701 number of observations (N=2) that we have for comparison. Due to potential variations in source
702 water locations feeding Bering Strait under high and low flow conditions, it is not clear that a 50%
703 increase in volume transport would increase to a commensurate change in the nutrient flux.
704 Nevertheless, the higher nutrient concentrations observed in 2012 are consistent with higher
705 salinities in this year and we hypothesize that changes in AW transport may have been primarily
706 responsible for both the salinity and nutrient differences. Given the large inter-annual variability in
707 the net Bering Strait transport, there appears potential for materially important interannual
708 changes to the Chukchi nutrient budget and the regional net productivity.
709 The Yukon discharge appeared to follow different pathways out of Norton Sound in the two
710 years (along the eastern shore of Bering Strait in 2012 and mostly trapped within Norton Sound or
711 spread to the west and south in 2013). These distributions conform to inter-annual differences in
712 the wind field (Figure 3) and the expected influence of Ekman transport (Danielson et al., 2014) and
713 suggest that the two years at least began the fall with very different distributions of the terrestrial
714 fresh water and associated lithogenic matter. Norton Sound has an average depth of ~40 m and
715 surface area of $\sim 3 \times 10^4$ km^2. For an estimated average summer salinity decrease of 2, there would
716 be approximately 80 km^3 of excess fresh water stored in the Sound, or about 40% of the annual
717 total Yukon discharge. Hence, some significant fraction of the Yukon's spring and summer discharge
718 likely remains on the Bering shelf by early fall. Sufficient winds can subsequently drive this
719 freshwater westward (Danielson et al., 2006; Danielson et al., 2012) and possibly even off the shelf,
720 where it would be effectively lost to the Arctic. The Yukon is generally considered an Arctic River
721 (Peterson et al., 2002) with all of its discharge feeding Bering Strait but a wind-mediated
722 redistribution of the coastal plume could impart a small (~ 5% of the annual Bering Strait

723 freshwater flux, Aagaard and Carmack, 1989) but possibly not negligible freshwater variability to
724 the Bering Strait throughflow.
725 It might seem that the shelf system of 2013 more closely resembled the shelf of three
726 decades ago, with the high ice concentrations in spring, the broad extent of CSWW and the cold ice
727 melt in the NE Chukchi. However, the September 2013 ice field was not nearly as extensive as was
728 normally found in the 1970s and 1980 and even 2013 nearly set a record for the lateness in
729 freezeup across the study region. Similarly, shelfbreak upwelling – a potential source for new
730 production both in the summer and fall (Pickart et al., 2013; Arrigo et al., 2014) – would be
731 associated with ACC reversals in Barrow Canyon and has likely increased in recent years. For all of
732 the above reasons we believe that the 2013 summer shelf does not provide a good analogue for the
733 cold shelf conditions in past decades.
734 As shown in Figure 2, the length in days of the seasonal transition is rapidly decreasing in
735 both spring and fall, so processes that depend on the presence of melting ice or partial ice cover
736 have less time to manifest. These could include under-ice phytoplankton blooms (e.g. Arrigo et al.,
737 2014), or ice as a platform for moving walrus (Jay et al., 2010). Eventually the system may reach a
738 new persistent balance rather than one of progressive change from year to year, because the
739 seasonal transition can eventually only decrease so far given the bounds of oceanic heat losses and
740 gains that are mediated by the solar cycle.
741
742 **5. Summary**
743 The data provided an unusual glimpse into the late summer temporal and spatial variability
744 in the water mass structure and characteristics, nutrient fields, and phytoplankton community on
745 the northern Bering and Chukchi shelves. We find that the wind field influenced water mass
746 distributions across the entire study region and it was likely responsible for at least a partial shut-
747 down of the ACC in 2013 on the NE Chukchi shelf that was associated with extensive MW and

748 CSWW and relatively large size phytoplankton. ACW were found all along the coast from Nunivak
749 Island to Point Barrow in 2012, but in response to the persistent wind of 2013 ACW was not found
750 north of Ledyard Bay. Instead, the 2013 NE Chukchi shelf was flooded with cold and fresh water
751 derived from ice melt that resided above cold and salty BCWW. Similarly, in the northern Bering
752 Sea, low-salinity coastal water from western Alaska were driven offshore to a greater extent in
753 2013, while in 2012 they were found more confined to shore and more prominently extended
754 northward along the coast through Bering Strait. Higher salinities in 2012 subsurface BCSW were
755 associated with higher nutrient concentrations and a higher overall phytoplankton standing crop
756 biomass that was dominated by small size phytoplankton. Nutrient and phytoplankton
757 distributions were both affected by water mass location and structure, which in turn reflected the
758 influence of geographic location, currents and winds. The observed and inferred flow field
759 differences suggest a different fate for pelagic production and the waters flowing north through
760 Bering Strait in these two strongly contrasting summers.
761
762 **6. Acknowledgements**
763 We thank the captain and crew of the Bering Explorer, and all of the Arctic Eis scientists
764 who helped carry this program forward, particularly Franz Mueter and Jared Weems for keeping us
765 all on track. Thanks to BOEM program managers Cathy Coon (Arctic Eis) and Warren Horowitz (NE
766 Chukchi circulation studies). Thanks to Rachel Potter for processing the HFR data, to Elizabeth
767 Dobbins for processing the surface drifter data, and to Eric Wisegarver and Peter Proctor for
768 nutrient analysis. Microstar 1-m drogue surface drifter data deployed at the nearshore locations in
769 2012 and 2013 were supported by the North Slope Borough-Shell Baseline Studies Program. The
770 offshore drifter deployments, BC2 subsurface mooring, Point Lay surface mooring, and HFR data
771 collections were supported by BOEM under contract #M12AC00008. This publication was partially
772 funded by the Joint Institute for the Study of the Atmosphere and Ocean (JISAO) under NOAA

773 Cooperative Agreement NA10OAR4320148, and is PMEL contribution number 4363, contribution
774 EcoFOCI-0845 to NOAA's Ecosystems and Fisheries-Oceanography, and JISAO contribution number
775 2446. S. Danielson was supported in part by NPRB project #1302 and NSF grant ARC 1108440.
776 Arctic Eis was funded under grants including the Coastal Impact Assistance Program
777 (AKDNR/USFWS), the University of Alaska Fairbanks 10-CIAP-010, and F12AF00188, Bureau of
778 Ocean Energy Management and the University of Alaska Fairbanks M12AC00009.
779

780 **7. References**

781 Aagaard, K., Coachman, L.K. and Carmack, E.C. 1981. On the halocline of the Arctic Ocean, Deep-Sea
782 Res., 28, 529-545.
783 Aagaard, K., Roach, A.T., and chumacher, J.D., 1985. On the wind-driven variability of the flow
784 through Bering Strait, *J. Geophys. Res.*, 90, 7213-7221.
785 Aagaard, K., Carmack, E.C., 1989. The role of sea ice and other fresh water in the Arctic circulation. J.
786 Geophys. Res. 94, 14485–14498.
787 Aagaard, K., Weingartner, T. J., Danielson, S. L., Woodgate, R. A., Johnson, G. C., Whitledge, T.E., 2006.
788 Some controls on flow and salinity in Bering Strait. Geophys. Res. Lett. 33, L19602,
789 doi:19610.11029/12006GL026612.
790 Arrigo, K.R., Perovich, D.K., Pickart, R.S., Brown, Z.W., van Dijken, G.L., Lowry, K.E., Mills, M.M.,
791 Palmer, M.A., Balch, W.M., Bates, N.R., Benitez-Nelson, C.R., Brownlee, E., Frey, K.E., Laney, S.R.,
792 Mathis, J., Matsuoka, A., Mitchell, B.G., Moore, G.W.K., Reynolds, R.A., Sosik, H.M., Swift, J.H., 2014.
793 Phytoplankton blooms beneath the sea ice in the Chukchi sea. Deep-Sea Res. II 105, 1-16.
794 10.1016/j.dsr2.2014.03.018.
795 Cavalieri, D. J., Parkinson, C.L., Gloersen, P. and Zwally, H., 1996, updated yearly. *Sea Ice
796 Concentrations from Nimbus-7 SMMR and DMSP SSM/I-SSMIS Passive Microwave Data.* [indicate
797 subset used]. Boulder, Colorado USA: NASA National Snow and Ice Data Center Distributed
798 Active Archive Center. http://dx.doi.org/10.5067/8GQ8LZQVL0VL.
799 Clement, J. L., Maslowski, W., Cooper, L.W., Grebmeier, J. M. and Walczowski, W.,2005. Ocean
800 circulation and exchanges through the northern Bering Sea: 1979– 2001, *Deep Sea Res. II*, 52,
801 3509–3540, doi:10.1016/j.dsr2.2005.09.010.
802 Coachman, L.K., Aagaard, K., Tripp, R.B., 1975. Bering Strait: The regional physical oceanography.
803 University of Washington Press, Seattle.

804 Coachman, L.K., 1993. On the flow field in the Chirikov Basin, *Cont. Shelf Res*., 13, 481-508.
805 Codispoti, L. A., Flagg, C., Kelly, V. and Swift, J.H., (2005), Hydrographic conditions during the 2002
806 SBI process experiments, Deep Sea Research Part II: Topical Studies in Oceanography, 52, 3199-
807 3226.
808 Cota, G.F., Pomeroy, L.R., Harrison, W.G., Jones, E.P., Peters, F. , Sheldon, W.M. , Weingartner, T.J.
809 1996. Nutrients, primary production and microbial heterotrophy in the southeastern Chukchi
810 Sea: Arctic summer nutrient depletion and heterotrophy, Marine Ecology Progress Series, 135,
811 247–258
812 Coyle, K.O., Konar, B., Blanchard, A, Highsmith, R.C., Carroll, J., Carroll M., Denisenko, S.G., Sirenko,
813 B.I., 2007. Potential effects of temperature on the benthic infaunal community on the
814 southeastern Bering Sea shelf: possible impacts of climate change. Deep Sea Research Part II:
815 Topical Studies in Oceanography 54, 2885–2905.
816 Danielson, S., 1996. Chukchi Sea Tidal Currents: Model and Observations. University of Alaska
817 Fairbanks Masters Thesis.
818 Danielson, S., and Kowalik, Z., 2005. Tidal currents in the St. Lawrence Island region, J. Geophys.
819 Res., 110, C10004, doi:10.1029/ 2004JC002463.Danielson, S., K. Aagaard, T. Weingartner, S.
820 Martin, P. Winsor, G. Gawarkiewicz, and D. Quadfasel, 2006. The St. Lawrence polynya and the
821 Bering shelf circulation: new observations that test the models, *J. Geophys. Res.,* J111, C09023,
822 doi:10.1029/2005JC003268.
823 Danielson, S., L. Eisner, T. Weingartner and K. Aagaard, 2011. Thermal and haline variability over
824 the central Bering Sea shelf: Seasonal and inter-annual perspectives. *Cont. Shelf Res*.,
825 doi:10.1016/j.csr.2010.12.010
826 Danielson, S., K. Hedstrom, K. Aagaard, T. Weingartner, and E. Curchitser, 2012a. Wind-induced
827 reorganization of the Bering shelf circulation, *Geophys. Res. Lett*., 39, L08601,
828 doi:10.1029/2012GL051231.
829 Danielson, S., T. Weingartner, K. Aagaard, J. Zhang, and R. Woodgate, 2012b. Circulation on the
830 central Bering Sea shelf, July 2008 to July 2010, *J. Geophys. Res*., 117, C10003,
831 doi:10.1029/2012JC008303.
832 Danielson, S.L., Weingartner, T.J., Hedstrom, K.S., Aagaard, K., Woodgate, R., Curchitser, E., Stabeno,
833 P.J., 2014. Coupled wind-forced controls of the Bering-Chukchi shelf circulation and the Bering
834 Strait throughflow: Ekman transport, continental shelf waves, and variations of the Pacific-
835 Arctic sea surface height gradient. Prog. Oceanogr. 125, 40-61.
836 http://dx.doi.org/10.1016/j.pocean.2014.04.006.

837 Dortch, Q., 1990. The interaction between ammonium and nitrate uptake in phytoplankton. Marine
838 ecology progress series. Oldendorf, 61(1), 183-201.
839 Feder, H.M., Jewett, S.C., 1981. Feeding interactions in the eastern Bering Sea with emphasis on the
840 benthos. In: Hood, D.W., Calder, J.A. (Eds.), The Eastern Bering Sea Shelf Oceanography and
841 Resources, vol. 2. U.S. Department of Commerce, NOAA, Rockville, pp. 1229–1261.
842 Frey, K. E., J. A. Maslanik, J. Clement Kinney, and W. Maslowski, 2014. Recent Variability in Sea Ice
843 Cover, Age and Thickness in the Pacific Arctic Region. In: J.M. Grebmeier and W. Maslowski
844 (eds.), The Pacific Arctic Region: Ecosystem Status 31, Springer and Trends in a Rapidly
845 Changing Environment, DOI 10.1007/978-94-017-8863-2_3,
846 Gawarkiewicz, G., Haney, J.C., Caruso, M.J., 1994. Summertime synoptic variability of frontal systems
847 in the northern Bering Sea. J. Geophys. Res. - Oceans 99, 7617-7625. 10.1029/94jc00259.
848 Gordon, L.I., J.C. Jennings Jr, A.A. Ross and J.M. Krest, 1994. A suggested protocol for continuous
849 flow automated analysis of seawater nutrients (phosphate, nitrate, nitrite and silicic acid) in the
850 WOCE Hydrographic Program and the Joint Global Ocean Fluxes Study. WHP Operations and
851 Methods. WOCE Hydrographic Program Office, Methods Manual 91-1, November
852 Grebmeier, J.M., McRoy, C.P., Feder, H.M., 1988. Pelagic–benthic coupling on the shelf of the
853 northern Bering and Chukchi Seas. I. Food supply source and benthic biomass. Marine Ecology
854 Progress Series 48, 57–67
855 Grebmeier, J.M., Overland, J.E., Moore, S.E., Farley, E.V., Carmack, E.C., Cooper, L.W., Frey, K.E., Helle,
856 J.H., McLaughlin, F.A., McNutt, S.L., 2006. A major ecosystem shift in the northern Bering Sea
857 Science 311, 1461-1464. 10.1126/science.1121365.
858 Grebmeier, J.M., Moore, S.E., Overland, J.E., Frey, K.E., Gradinger, R., 2010. Biological response to
859 recent Pacific Arctic sea ice retreats. Eos, Trans., AGU 91, 161-162.
860 Grebmeier, J.M., Bluhm, B.A., Cooper, L.W., Danielson, S.L., Arrigo, K.R., Blanchard, A.L., Clarke, J.T.,
861 Day, R.H., Frey, K.E., Gradinger, R.R., Kędra, M., Konar, B., Kuletz, K.J., Lee, S.H., Lovvorn, J.R.,
862 Norcross, B.L., Okkonen, S.R., 2015. Ecosystem characteristics and processes facilitating
863 persistent macrobenthic biomass hotspots and associated benthivory in the Pacific Arctic. Prog.
864 Oceanogr. 136, 92-114. http://dx.doi.org/10.1016/j.pocean.2015.05.006.
865 Hill, V., Cota, G., 2005. Spatial patterns of primary production on the shelf, slope and basin of the
866 Western Arctic in 2002. Deep-Sea Res. II 52, 3344-3354.
867 http://dx.doi.org/10.1016/j.dsr2.2005.10.001.

Hirano, D., Y. Fukamachi, E. Watanabe, K. I. Ohshima, K. Iwamoto, A. R. Mahoney, H. Eicken, D. Simizu, and T. Tamura, 2016. A wind-driven, hybrid latent and sensible heat coastal polynya off Barrow, Alaska, J. Geophys. Res. Oceans, 121, 980–997, doi:10.1002/2015JC011318.

Hunt G.L., Harrison N.M., 1990. Foraging habitat and prey taken by least auklets at King Island, Alaska. Mar Ecol Prog Ser 65:141–150

Iken, K., Bluhm, B.A., Dunton, K., 2010. Benthic food web structure serves as indicator of water mass properties in the southern Chukchi Sea. Deep Sea Research Part II: Topical Studies in Oceanography 57, 71–85

Jay, C. V., J. M. Grebmeier, A. S. Fischbach, T. L. McDonald, L. W. Cooper, and F. Hornsby. 2014. Pacific walrus (*Odobenus rosmarus divergens*) resource selection in the northern Bering Sea. PLoS One 9(4):e93035. doi:10.1371/journal.pone.0093035

Jay, C. V., A. S. Fischbach, and A. A. Kochnev. 2012. Walrus areas of use in the Chukchi Sea during sparse sea ice cover. Marine Ecology Progress Series 468:1-13. doi:10.3354/meps10057

Jay, C.V., Udevitz, M.S., Kwok, R., Fischbach, A.S., Douglas, D.C., 2010. Divergent movements of walrus and sea ice in the northern Bering Sea. Mar. Ecol. Prog. Ser. 407, 293-302. 10.3354/meps08575.

Kinder, T.H., Chapman, D.C., Whitehead, J.A., 1986. Westward intensification of the mean circulation on the Bering Sea Shelf. J. Phys. Oceanogr. 16, 1217-1229. 10.1175/1520-0485(1986)016<1217:wiotmc>2.0.co;2.

Kwok, R., and D. A. Rothrock, 2009. Decline in Arctic sea ice thickness from submarine and ICESat records: 1958–2008. Geophys Res Lett 36:L15501. doi: 10.1029/2009GL039035

Logerwell, E., Busby, M., Carothers, C., Cotton, S., Duffy-Anderson, J., Farley, E., Goddard, P., Heintz, R., Holladay, B., Horne, J., Johnson, S., Lauth, B., Moulton, L., Neff, D., Norcross, B., Parker-Stetter, S., Seigle, J., Sformo, T., 2015. Fish communities across a spectrum of habitats in the western Beaufort Sea and Chukchi Sea. Prog. Oceanogr. 136, 115-132. http://dx.doi.org/10.1016/j.pocean.2015.05.013.

Lu, K. F., T. J. Weingartner, S. L. Danielson, P. Winsor, E. L. Dobbins, K. Martini, and H. Statscewich, (in revision), Lateral mixing across ice meltwater fronts of the Chukchi Sea shelf, in revision for *Geophys. Res. Lett.*

Luchin, V. and Panteleev, G., 2014. Thermal regimes in the Chukchi Sea from1941 to 2008. Deep Sea Res. II. 109, 14-26.

Mann, K. H. & Lazier, J. R. N., 1991. *Dynamics of Marine Ecosystems*, Blackwell.

R.F.C. Mantoura and E.M.S. Woodward, 1983. Optimization of the indophenol blue method for the automated determination of ammonia in estuarine waters. Estuar. Coast. Shelf Sci., 17, pp. 219–224

Marsh, J., F. J. Mueter, K. Iken, S. L. Danielson, submitted, Ontogenetic, spatial and temporal variation in trophic roles of Chukchi Sea fishes, Deep-Sea Res. II

Martin, S., Drucker, R., 1997. The effect of possible Taylor columns on the summer ice retreat in the Chukchi Sea. J. Geophys. Res. - Oceans 102, 10473–10482.

Martini, K. I., P. J. Stabeno, C. Ladd, P. Winsor, T. J. Weingartner, C. W. Mordy, and L. B. Eisner 2016., Dependence of subsurface chlorophyll on seasonal water masses in the Chukchi Sea, J. Geophys. Res. Oceans, 121, doi:10.1002/2015JC011359

Moran, K., and J.W. Farrell. 2011. US Arctic research policy. Oceanography 24(3):18–25, http://dx.doi.org/10.5670/oceanog.2011.51.

Mueter, F.J., Litzow, M.A., 2008. Sea ice retreat alters the biogeography of the Bering Sea continental shelf. Ecological Applications 18, 309-320. doi: 10.1890/07-0564.1.

National Research Council (NRC), 2014, The Arctic in the Anthropocene, Emerging Research Questions. Committee on Emerging Research Questions in the Arctic, Polar Research Board, Division on Earth and Life Studies, H. Huntington and S. Pfirman, co-chairs, 224 pp.,

Parsons TR, Maita Y, Lalli CM, 1984. A manual of biological and chemical methods for seawater analysis. Pergamon Press, Oxford

Peterson, B. J., Holmes, R. M., McClelland, J.W., Vorosmarty, C. V., Lammers, R. B., Shiklomanov,A. I., Shiklomanov, I. A., and Rahmstorf, S.: 2002, 'Increasing river discharge to the ArcticOcean', Science 298, 2171–2173.

Pickart, R.S., L.M. Schulze, G.W.K. Moore, M.A. Charette, K. R. Arrigo, G. van Dijken, S.L. Danielson, 2013. Long-term trends of upwelling and impacts on primary productivity in the Alaskan Beaufort Sea, Deep Sea Res. Part I: Oceanographic Research Papers, Volume 79, http://dx.doi.org/10.1016/j.dsr.2013.05.003.

Pinchuk A.I. and L. B. Eisner. submitted. Spatial heterogeneity in zooplankton distribution in the eastern Chukchi Sea as a result of large-scale interactions of water masses, DSR-II Arctic Eis special issue.

Polashenski, C., D.Perovich, and Z.Courville. 2012. The mechanisms of sea ice melt pond formation and evolution, J. Geophys. Res., 117, C01001, doi: 10.1029/2011JC007231.

Overland, J.E., Roach, A.T., 1987. Northward flow in the Bering and Chukchi Seas. J. Geophys. Res. - Oceans 92, 7097-7105.

Overland, J. E., P. J. Stabeno, and S. Salo (1996), Direct evidence for northward flow on the northwestern Bering Sea shelf, J. Geophys. Res., 101, 8971–8976, doi:10.1029/96JC00205.

Roach, A.T., Aagaard, K., Pease, C.H., Salo, S.A., Weingartner, T., Pavlov, V., Kulakov, M., 1995. Direct measurements of transport and water properties through Bering Strait. J. Geophys. Res. 100, 18443-18457.

Sigler, M.F., F.J. Mueter, B. A. Bluhm, M. S. Busby, E. D. Cokelet , S.L. Danielson, A. De Robertis, L. B. Eisner, E.V. Farley, K. Iken, K. J. Kuletz, R. R. Lauth, E.A. Logerwell, A.I. Pinchuk, Summer zoogeography 1 of the northern Bering and Chukchi seas, submitted to DSR-II Arctic Eis special issue

Spall, M. A., 2007. Circulation and water mass transformation in a model of the Chukchi Sea, *J. Geophys. Res.,* 112, C05025, doi:10.1029/2005JC003364.

Sambrotto, R.N., J.J. Goering, and C.P. McRoy, 1984. Large yearly production of phytoplankton in the western Bering Strait. Science. 225:1147-1150.

Stabeno, P., Kachel, N., Ladd, C., Martini, K.I., Mordy, C., accepted. Currents and transport on the Chukchi Shelf: 2010 - 2014. Cont. Shelf Res.

Shimada K, Kamoshida T, Itoh M, Nishino S, Carmack E, McLaughlin F, Zimmerman S, Proshutinsky A (2006) Pacific Ocean inflow: influence on catastrophic reduction of sea ice cover in the Arctic Ocean. Geophys Res Lett 33:L08605. doi:10.1029/2005GL025624

Springer, A.M., 1988. The paradox of pelagic food webs on the Bering–Chukchi continental shelf. Dissertation, University of Alaska Fairbanks

Springer, A.M. and C.P. McRoy. 1993. The paradox of pelagic food webs in the northern Bering Sea. III. Patterns of primary production. Cont. Shelf Res. 13:575-579.

Stabeno, P.J., Kachel, N.B., Sullivan, M., Whitledge, T.E., 2002. Variability of physical and chemical characteristics along the 70-m isobath of the southeast Bering Sea. Deep-Sea Research Part II 49, 5931–5943

Stigebrandt, A., 1984. The North Pacific: A global-scale estuary. J. Phys. Oceanogr. 14, 464-470. 10.1175/1520-0485(1984)014<0464:TNPAGS>2.0.CO;2.

Timmermans, M.-L., A. Proshutinsky, E. Golubeva, J. M. Jackson, R. Krishfield, M. McCall, G. Platov, J. Toole, W. Williams, T. Kikuchi, and S. Nishino (2014), Mechanisms of Pacific Summer Water variability in the Arctic's Central Canada Basin, J. Geophys. Res. Oceans, 119, 7523-7548, doi:10.1002/2014JC010273

Walsh, J.J., McRoy, C.P., Coachman, L.K., Goering, J.J., Nihoul, J.J., Whitledge, T.E., Blackburn, T.H., Parker, P.L., Wirick, C.D., Shuert, P.G., Grebmeier, J.M., Springer, A.M., Tripp, R.D., Hansell, D.A.,

965 Djenidi, S., Deleersnijder, E., Henriksen, K., Lund, B.A., Andersen, P., Mullerkarger, F.E., Dean, K.,
966 1989. Carbon and nitrogen cycling within the Bering Chukchi Seas - source regions for organic-
967 matter effecting AOU demands of the Arctic Ocean. Prog. Oceanogr. 22, 277-359. 10.1016/0079-
968 6611(89)90006-2.
969 Weingartner, T., Aagaard, K., Woodgate, R., Danielson, S., Sasaki, Y., Cavalieri, D., 2005. Circulation
970 on the north central Chukchi Sea shelf. Deep-Sea Res. II 52, 3150-3174.
971 Weingartner, T.J., Danielson, S., Sasaki, Y., Pavlov, V., Kulakov, M., 1999. The Siberian Coastal
972 Current: A wind- and buoyancy-forced Arctic coastal current. J. Geophys. Res. 104, 29697–
973 29713. Weingartner, T., Aagaard, K., Woodgate, R., Danielson, S., Sasaki, Y., Cavalieri, D., 2005.
974 Circulation on the north central Chukchi Sea shelf. Deep-Sea Res. II 52, 3150-3174.
975 Winsor, P., and D. C. Chapman, 2004. Pathways of Pacific water across the Chukchi Sea: a numerical
976 model study. *J. Geophys. Res*., 109 (C3), 10.1029/2003JC001962.
977 Woodgate, R.A., Aagaard, K., Weingartner, T.J., 2005a. A year in the physical oceanography of the
978 Chukchi Sea: Moored measurements from autumn 1990-1991. Deep-Sea Res. II 52, 3116-3149.
979 Woodgate, R.A., Aagaard, K., Weingartner, T.J., 2005b. Monthly temperature, salinity, and transport
980 variability of the Bering Strait through flow. Geophys. Res. Lett. 32. L04601,
981 doi:10.1029/2004GL021880.
982 Woodgate, R., Stafford, K.M., Prahl, F.G., 2015. A Synthesis of Year-round Interdisciplinary Mooring
983 Measurements in the Bering Strait (1990-2014) and the RUSALCA years (2004-2011).
984 Oceanography 28(3), 46-67.
985 Woodgate, R.A., Weingartner, T.J., Lindsay, R., 2012. Observed increases in Bering Strait oceanic
986 fluxes from the Pacific to the Arctic from 2001 to 2011 and their impacts on the Arctic Ocean
987 water column. Geophys. Res. Lett. 39. L24603, doi: 10.1029/2012GL054092.
988

8. Table and Figure Captions

Table 1. Water mass temperature and salinity bounds and defining characteristics. Abbreviations include ACW = Alaskan coastal water, AtlW = Atlantic Water, AW = Anadyr Water, BSSW = Bering Shelf Summer Water, BCSW = Bering-Chukchi Summer Water, BCWW = Bering-Chukchi Winter Water, BSWW = Bering Shelf Winter Water, CSSW = Chukchi Shelf Summer Water, and CSWW = Chukchi Shelf Winter Water.

Table 2. Mean surface and near-bottom T, S and nutrients (μM) by water mass, year and number of samples (N). Nutrients include nitrite (NO_2), nitrate (NO_3), ammonium (NH_4), silicic acid (Si), and phosphate (PO_4). Water mass abbreviations as in Table 1. One-way ANOVA used for comparisons between years for each water mass for natural log transformed nutrient data and untransformed T and S. * indicates significantly higher ($P< 0.05$) in that year.

Table 3. Mean integrated Chla (IntChla, mg m^{-2}) by water mass (WM) structure and year. Water masses as defined in Table 1. One-way ANOVA used for comparisons between years within each water mass combination for natural log transformed integrated Chla data. * indicates significantly higher ($P< 0.05$) in that year.

Figure 1. Study region map with bathymetric depths (200, 80, 45, 35, and 25 m isobaths), place names and typical flow pathways. Abbreviations include NI = Nunivak Island, SLI = St. Lawrence Island, WI = Wrangel Island, KS = Kotzebue Sound, PB = Peard Bay. Mean flow pathways are color coded to denote current systems and/or typical water mass pathways: Yellow = Bering Slope Current and Beaufort Gyre; Black = Alaskan Coastal Current; Brown = Siberian Coastal Current; Purple = pathways of Bering shelf, Anadyr, and Chukchi shelf waters. Panels on the right hand side show the Arctic Eis station locations for 2012 and 2013. Full CTD hydrographic, nutrient and

phytoplankton sampling occurred at stations with squares, while only CTD sampling occurred at stations marked with an "x". Mooring BC2 location is marked with a red circle.

Figure 2 a: Sea ice concentrations over the region 60-72 °N and 170-157 °W for 1979-2014, showing the envelope of daily ice concentration ranges for first (blue, 1979-1996) and second (red, 1997-2014) halves of the period of record and the region of overlap between the two periods (purple). Daily ice concentrations for 2012 and 2013 are shown in red and blue, respectively. **b**: Number of days for the same region to transform from ice-covered (> 80%) to ice-free (< 20%) conditions in the spring/summer (red), and vice-versa in the fall/winter (blue). Spring $r^2 = 0.30$ and fall $r^2 = 0.29$ and $p < 0.001$ for both.

Figure 3. Monthly average sea level pressure contours (mbars) for August (left) and September (right) in 2012 (top) and 2013 (bottom) from the NCEP-NCAR Reanalysis.

Figure 4. Meteorological measurements from a surface buoy deployed offshore of Pt. Lay in 2012 (blue) and 2013 (red). From top to bottom, panels depict: 2 m air temperature (°C), 1 m depth water temperature (°C), integrated solar radiation (W m^{-2}), sea level pressure (mbar), and the east (U, m s^{-1}) and north (V m s^{-1}) components of the wind. In both years the Arctic Eis cruise operated in the Chukchi Sea from 10 August through the first week of September, working from south to north.

Figure 5. Mean monthly surface currents as measured by HFR installations at Point Lay, Wainwright, and Barrow in August and September 2012 and 2013. Note that incomplete coverage severely biases August 2013 due to missing data.

Figure 6. Surface (1-m) drogued satellite-tracked drifters deployed over 10-24 August 2012 (left) and 17-24 August 2013 (right). Color denotes the date of each location fix. Black dots locate the deployment sites.

Figure 7. Theta-S diagrams for 2012 (left) and 2013 (right). Contours show sigma-theta isolines with a contour interval of 1 kg m^{-3}. Data points are colored (see inset) by region: northern Chukchi shelf are red, southern Chukchi shelf are black and northern Bering shelf are blue. See Table 1 for water mass abbreviation definitions. The freezing point for seawater is shown by the dashed lines.

Figure 8. Distribution of water masses in 2012 (top row) and 2013 (bottom row). Colors denote the number of 1-m averaged data points found in each water column profile: 1-2 (green), 3-10 (blue) and more than 10 (red). No marker is displayed at stations that did not observe the corresponding water mass. See Table 1 for water mass abbreviation definitions. AtlW was found only at the easternmost station, near Point Barrow, in 2013.

Figure 9. Temperature (left four panels) and salinity (right four panels) within 10 m of the surface (top row) and near the seafloor, within 5 m of CTD cast deepest measurement (bottom row), for 2012 and 2013.

Figure 10. Stratification and fronts in 2012 (top) and 2013 (bottom). Left column shows the difference between the near-surface and near bottom water density. Middle column shows the magnitude of the near-surface horizontal density gradient and the right column shows the magnitude of the near-bottom horizontal density gradient.

Figure 11. Nutrient concentrations close to the surface (10 m) for 2012 (top row) and 2013 (bottom row). From left to right, the panels show NO_3, NH_4, SiO_4, and PO_4. Black boxes in nitrate plots denote benthic hotspot regions DBO-2 in Chirikov Basin and DBO-3 offshore of Point Hope, DB4 near Hanna Shoal, and DB5 at Barrow Canyon.

Figure 12. As in Figure 11, but for nutrients close to the seafloor.

Figure 13. Nutrients integrated through the water column for Chukchi Sea only at stations sampled in both 2012 (top row) and 2013 (bottom row). From left to right, the panels show NO3, NH4, SiO4, and PO4.

Figure 14. Surface chlorophyll a (mg m^{-3}) from discrete samples for 2012 (left) and 2013 (right). Black boxes denote benthic hotspot regions DBO-2 in Chirikov Basin and DBO-3 offshore of Point Hope, DB4 near Hanna Shoal, and DB5 at Barrow Canyon.

Figure 15. Total, large fraction (> 10 μm) and small fraction (<10 μm) water column integrated chlorophyll a (mg Chla m^{-2}) for 2012 (top) and 2013 (bottom). No size fraction data exist south of Bering Strait in 2013. Black boxes denote benthic hotspot regions DBO-2 in Chirikov Basin, DBO-3 offshore of Point Hope, DBO-4 near Hanna Shoal, and DB5 at Barrow Canyon.

9. **Tables**

Table 1. Water mass temperature and salinity bounds and defining characteristics. Abbreviations include ACW = Alaskan coastal water, AtlW = Atlantic Water, AW = Anadyr Water, BSSW = Bering Shelf Summer Water, BCSW = Bering-Chukchi Summer Water, BCWW = Bering-Chukchi Winter Water, BSWW = Bering Shelf Winter Water, CSSW = Chukchi Shelf Summer Water, and CSWW = Chukchi Shelf Winter Water.

Water Mass	Temperature Limits	Salinity Limits	Characteristics
ACW	7 < T < 12	20 < S < 32	The warmest and freshest water observed in the Arctic Eis surveys. Influenced by the fresh coastal discharges from Alaskan rivers and the ability for incident solar radiation to exert a proportionally larger warming in shallow, turbid water columns.
BSWW CSWW	-2 < T < 0	30 < S < 33.5	Cold water remnant from the previous winter's cooling, ice formation, and brine rejection. Together, these water masses comprise the **BCWW**.
AW BSSW CSSW	0 < T < 7	30 < S < 33.5	Water of intermediate temperature and salinity that have warmed since the previous winter or that have advected into the study domain from the Bering Sea continental slope and through the Gulf of Anadyr. Together, these water masses comprise the **BCSW**.
MW	-2 < T < 7	25 < S < 30	Relatively cool and fresh water influenced by sea ice melt. Can directly mix with summer shelf water, coastal water, or winter water.
AtlW	-2 < T < 1	33.5 < S < 35	Relatively saline water that originate in the North Atlantic and typically reside at depths below the Arctic Ocean's cold halocline. This water mass is characterized by a subsurface temperature maximum at about 300-600 m.

Table 2. Mean surface and near-bottom T, S and nutrients (μM) by water mass, year and number of samples (N). Nutrients include nitrite (NO_2), nitrate (NO_3), ammonium (NH_4), silicic acid (Si), and phosphate (PO_4). Water mass abbreviations as in Table 1. One-way ANOVA used for comparisons between years for each water mass for natural log transformed nutrient data and untransformed T and S. * indicates significantly higher ($P< 0.05$) in that year.

Layer	Year	Water Mass	N	T	S	NO_2	NO_3	NH_4	Si	PO_4
Surface	2012	MW	12	2.74	29.27*	0.01	0.72*	0.54*	8.93*	0.52*
Surface	2013	MW	16	1.78	27.93	0.01	0.04	0.12	3.41	0.35
Surface	2012	BCSW	44	5.33	31.16	0.03	1.27	0.58*	7.25*	0.54*
Surface	2013	BCSW	25	4.87	31.36	0.04	1.26	0.38	5.12	0.43
Surface	2012	ACW	40	8.17	29.77	0.02	0.13	0.54*	8.92	0.48*
Surface	2013	ACW	52	8.79*	29.64	0.02	0.27	0.22	7.77	0.39
near-bottom	2012	BSWW	1	-0.07	32.38	0.14	11.26	1.66	12.53	1.34*
near-bottom	2013	BSWW	6	-0.61	31.38	0.08	2.3	1.31	12.3	0.93
near-bottom	2012	CSWW	17	-0.92*	32.96*	0.14	7.36	3.11	21.86	1.56
near-bottom	2013	CSWW	24	-1.3	32.59	0.13	7.07	2.47	20.53	1.37
near-bottom	2012	BCSW	54	3.47	32.03*	0.08*	3.10*	2.06*	12.72*	0.94*
near-bottom	2013	BCSW	44	4.01	31.48	0.06	1.81	1.22	8.72	0.66
near-bottom	2012	ACW	25	8.35	29.9	0.04	0.2	1.08*	9.48	0.57
near-bottom	2013	ACW	18	9.16*	29.78	0.03	0.23	0.33	12.84	0.52

Table 3. Mean integrated Chla (IntChla, mg m^{-2}) by water mass (WM) structure and year. Water masses as defined in Table 1. One-way ANOVA used for comparisons between years within each water mass combination for natural log transformed integrated Chla data. * indicates significantly higher ($P < 0.05$) in that year.

Year	WM Surface	WM Bottom	IntChla	N
2012	MW	CSWW	43.88	17
2013	MW	CSWW	24.60	16
2012	MW	BCSW	31.34	2
2013	MW	BCSW	N/A	0
2012	BCSW	BSWW	39.57	1
2013	BCSW	BSWW	N/A	0
2012	BCSW	CSWW	18.51	9
2013	BCSW	CSWW	14.17	8
2012	BCSW	BCSW	61.94	37
2013	BCSW	BCSW	102.29	18
2012	ACW	BSWW	N/A	0
2013	ACW	BSWW	32.53	6
2012	ACW	BCSW	33.90*	15
2013	ACW	BCSW	16.82	28
2012	ACW	ACW	32.56*	25
2013	ACW	ACW	15.88	18

10. Figures

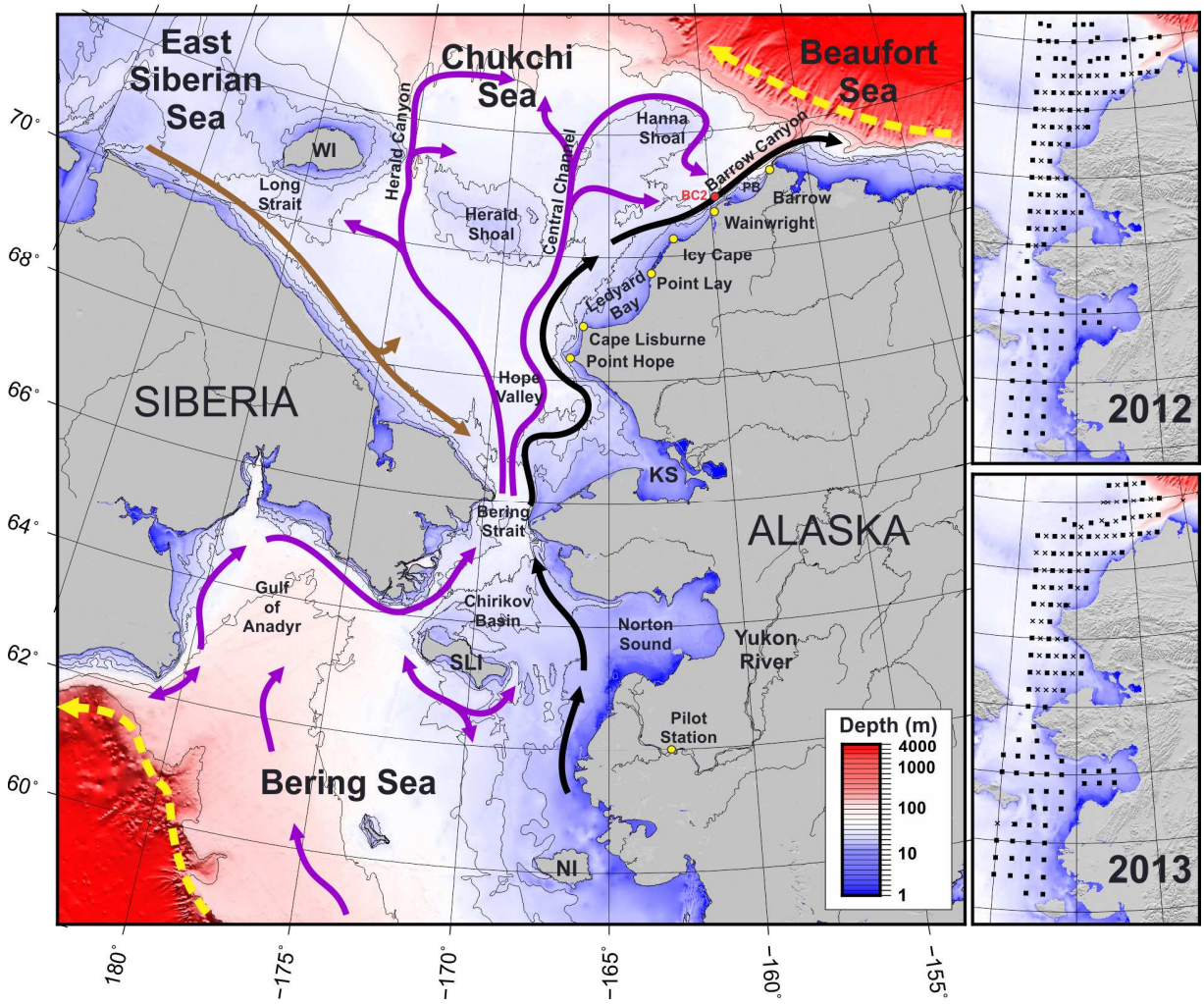

Figure 1. Study region map with bathymetric depths (200, 80, 45, 35, and 25 m isobaths), place names and typical flow pathways. Abbreviations include NI = Nunivak Island, SLI = St. Lawrence Island, WI = Wrangel Island, KS = Kotzebue Sound, PB = Peard Bay. Mean flow pathways are color coded to denote current systems and/or typical water mass pathways: Yellow = Bering Slope Current and Beaufort Gyre; Black = Alaskan Coastal Current; Brown = Siberian Coastal Current; Purple = pathways of Bering shelf, Anadyr, and Chukchi shelf waters. Panels on the right hand side show the Arctic Eis station locations for 2012 and 2013. Full CTD hydrographic, nutrient and

phytoplankton sampling occurred at stations with squares, while only CTD sampling occurred at stations marked with an "x". Mooring BC2 location is marked with a red circle.

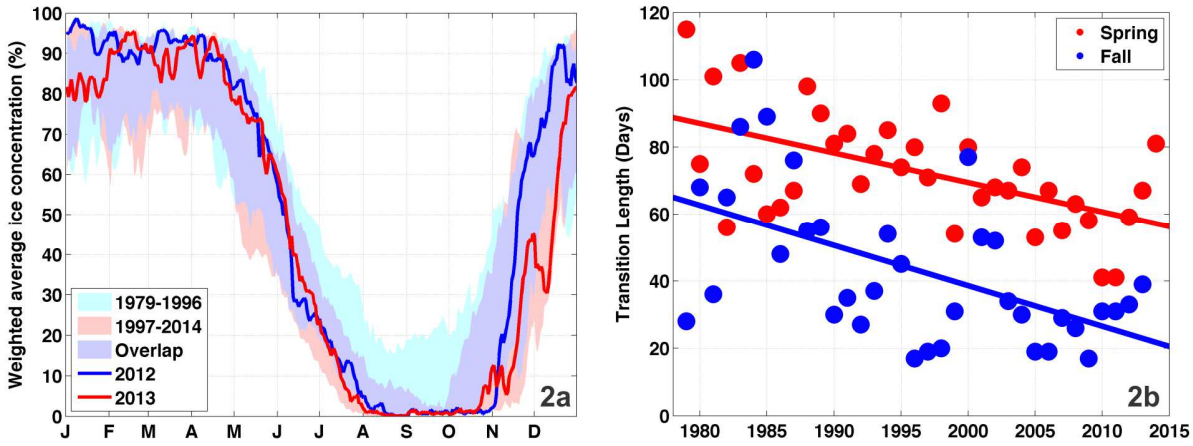

Figure 2. a: Sea ice concentrations over the region 60-72 °N and 170-157 °W for 1979-2014, showing the envelope of daily ice concentration ranges for first (blue, 1979-1996) and second (red, 1997-2014) halves of the period of record and the region of overlap between the two periods (purple). Daily ice concentrations for 2012 and 2013 are shown in red and blue, respectively. **b**: Number of days for the same region to transform from ice-covered (> 80%) to ice-free (< 20%) conditions in the spring/summer (red), and vice-versa in the fall/winter (blue). Spring $r^2 = 0.30$ and fall $r^2 = 0.29$ and $p < 0.001$ for both.

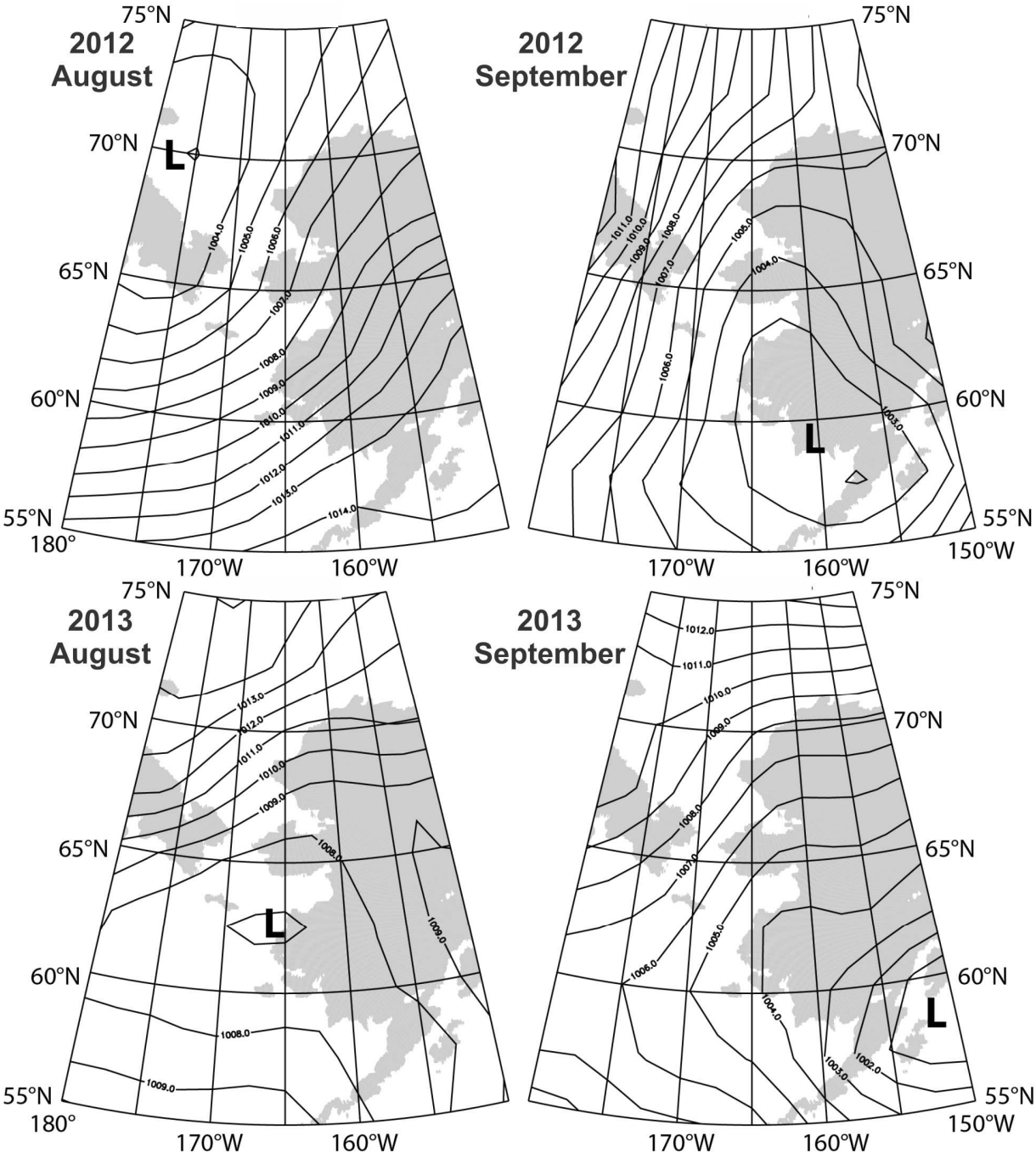

Figure 3. Monthly average sea level pressure contours (mbars) for August (left) and September (right) in 2012 (top) and 2013 (bottom) from the NCEP-NCAR Reanalysis.

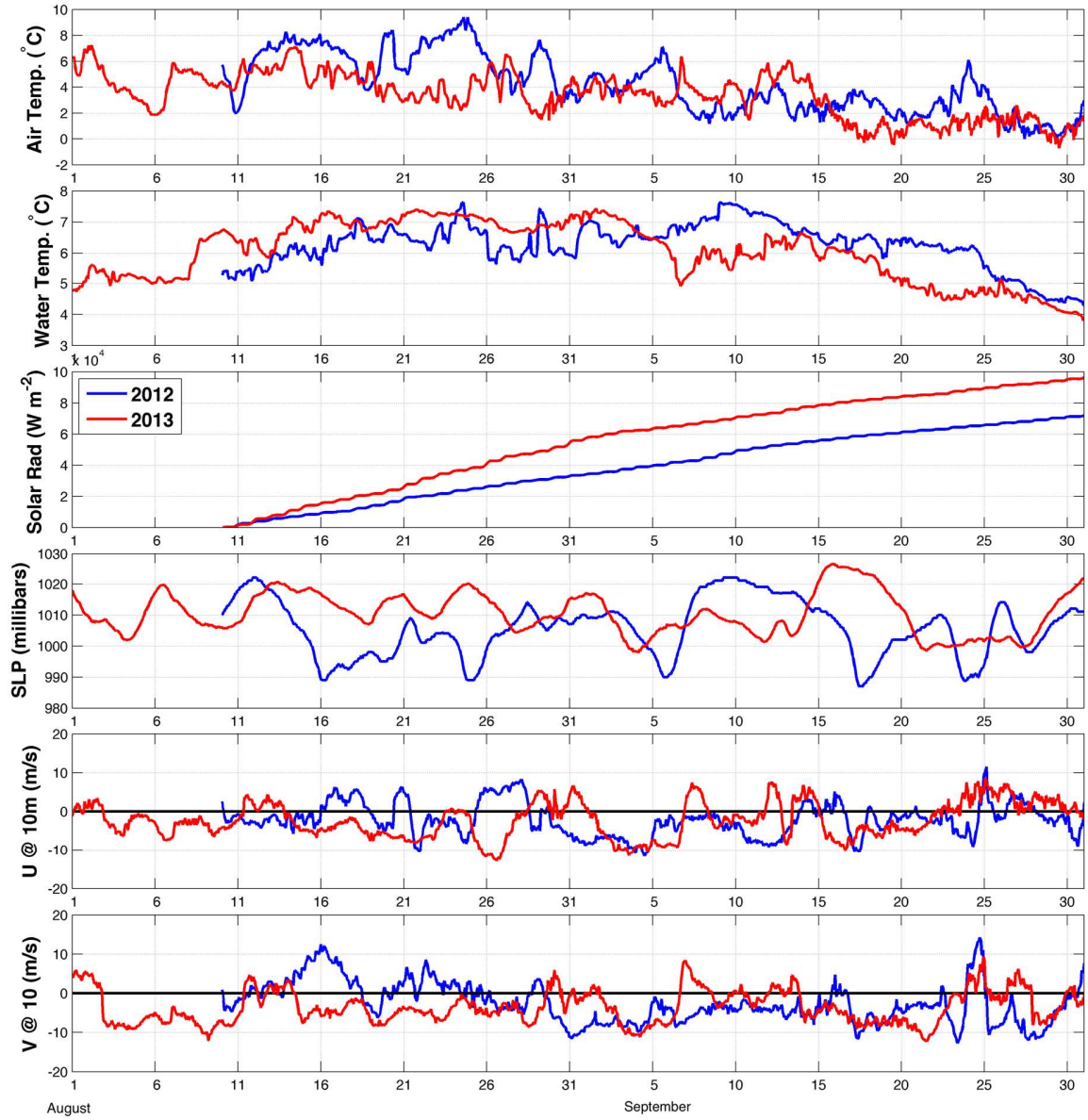

1143

1144 **Figure 4.** Meteorological measurements from a surface buoy deployed offshore of Pt. Lay in 2012

1145 (blue) and 2013 (red). From top to bottom, panels depict: 2 m air temperature (°C), 1 m depth

1146 water temperature (°C), integrated solar radiation (W m^{-2}), sea level pressure (mbar), and the east

1147 (U, m s^{-1}) and north (V m s^{-1}) components of the wind. In both years the Arctic Eis cruise operated in

1148 the Chukchi Sea from 10 August through the first week of September, working from south to north.

1149

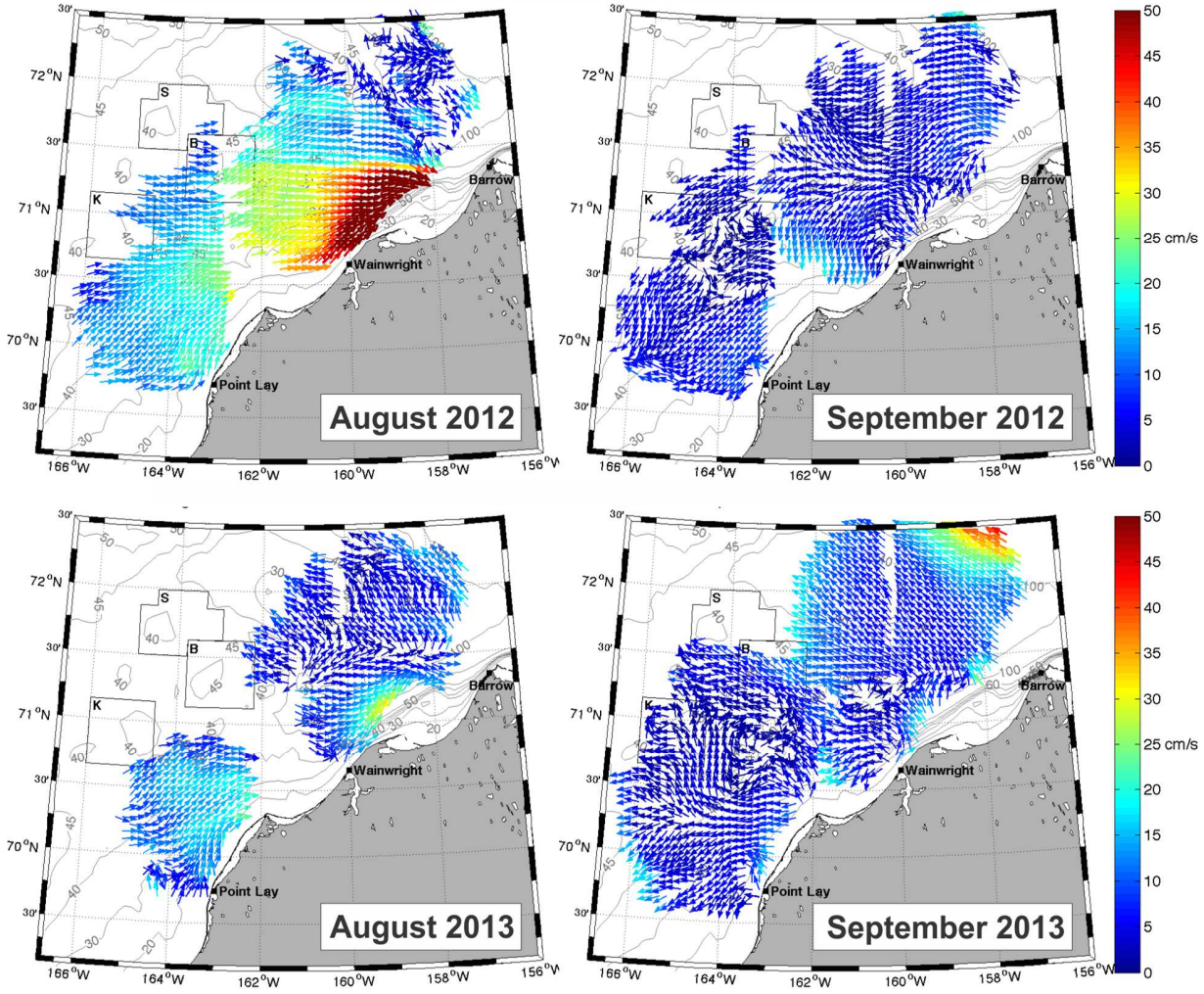

Figure 5. Mean monthly surface currents as measured by HFR installations at Point Lay, Wainwright, and Barrow in August and September 2012 and 2013. Note that incomplete coverage severely biases August 2013 due to missing data.

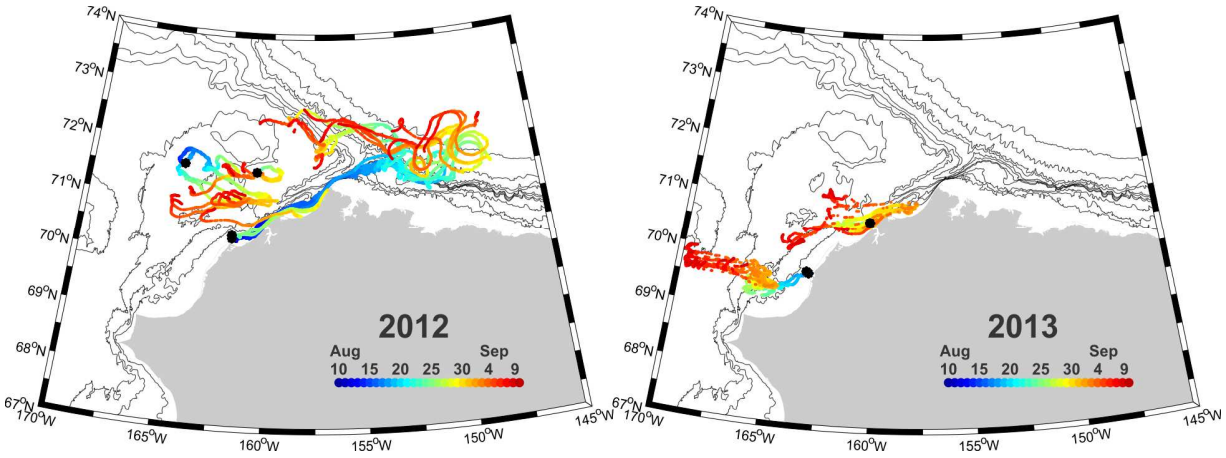

Figure 6. Surface (1-m) drogued satellite-tracked drifters deployed over 10-24 August 2012 (left) and 17-24 August 2013 (right). Color denotes the date of each location fix. Black dots locate the deployment sites.

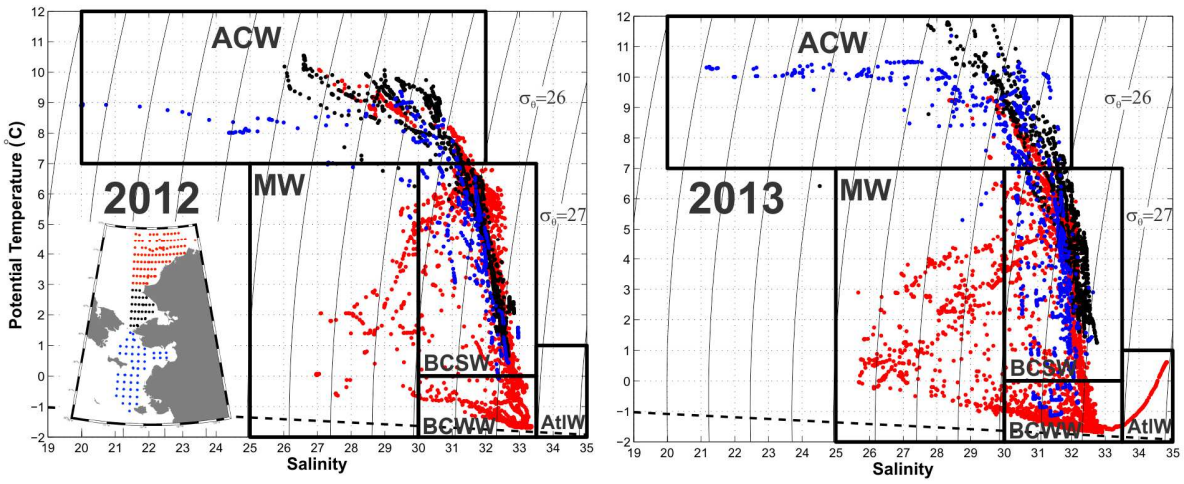

Figure 7. Theta-S diagrams for 2012 (left) and 2013 (right). Contours show sigma-theta isolines with a contour interval of 1 kg m^{-3}. Data points are colored (see inset) by region: northern Chukchi shelf are red, southern Chukchi shelf are black and northern Bering shelf are blue. See Table 1 for water mass abbreviation definitions. The freezing point for seawater is shown by the dashed lines.

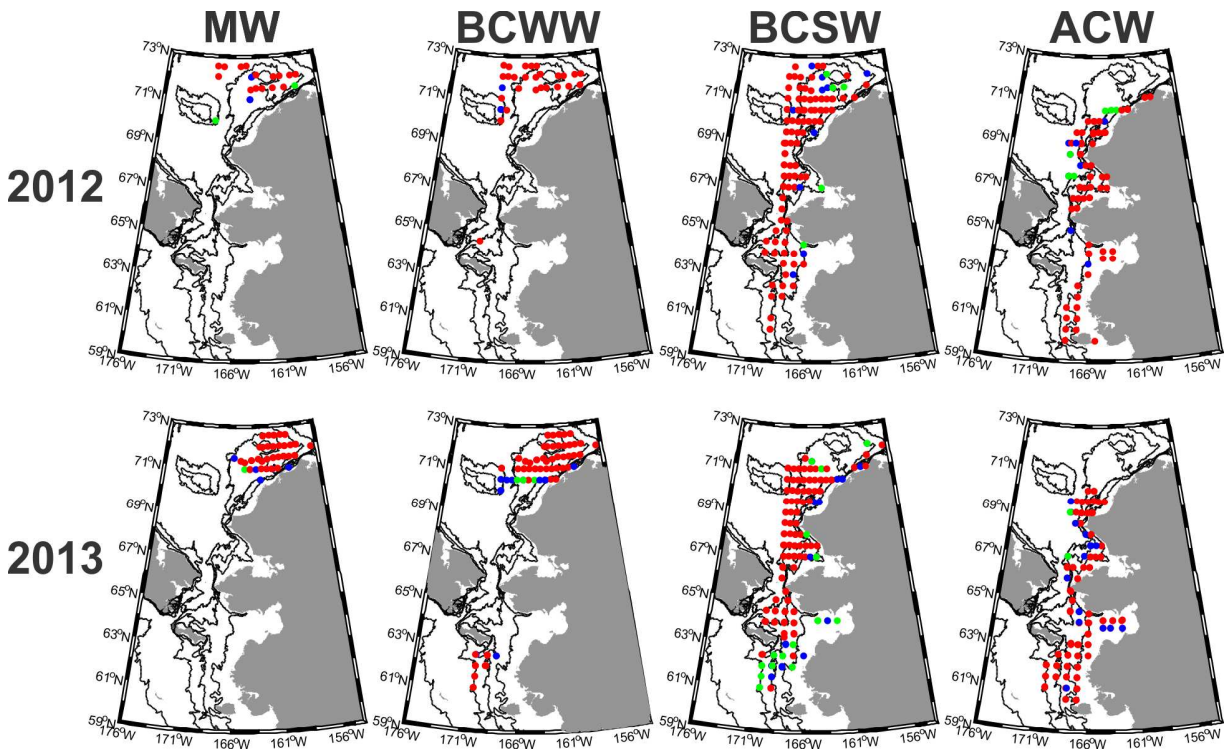

Figure 8. Distribution of water masses in 2012 (top row) and 2013 (bottom row). Colors denote the number of 1-m averaged data points found in each water column profile: 1-2 (green), 3-10 (blue) and more than 10 (red). No marker is displayed at stations that did not observe the corresponding water mass. See Table 1 for water mass abbreviation definitions. AtlW was found only at the easternmost station, near Point Barrow, in 2013.

.

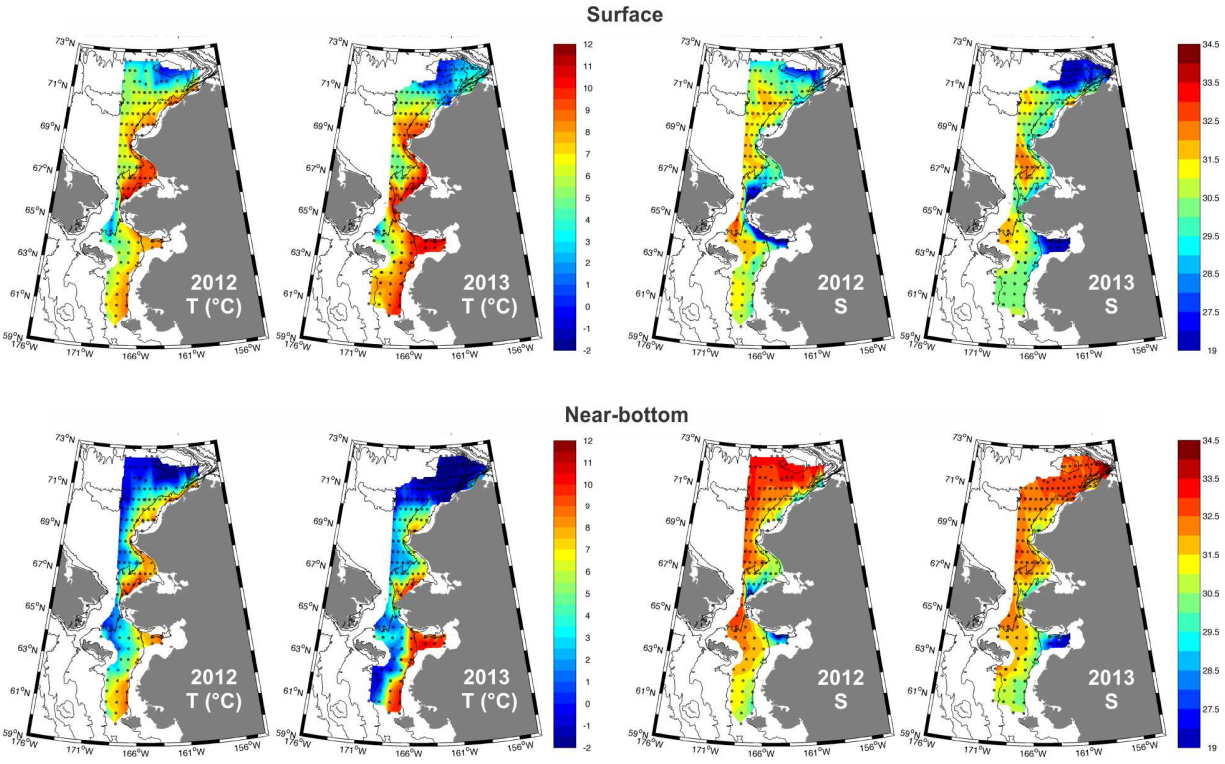

Figure 9. Temperature (left four panels) and salinity (right four panels) within 10 m of the surface (top row) and near the seafloor, within 5 m of CTD cast deepest measurement (bottom row), for 2012 and 2013.

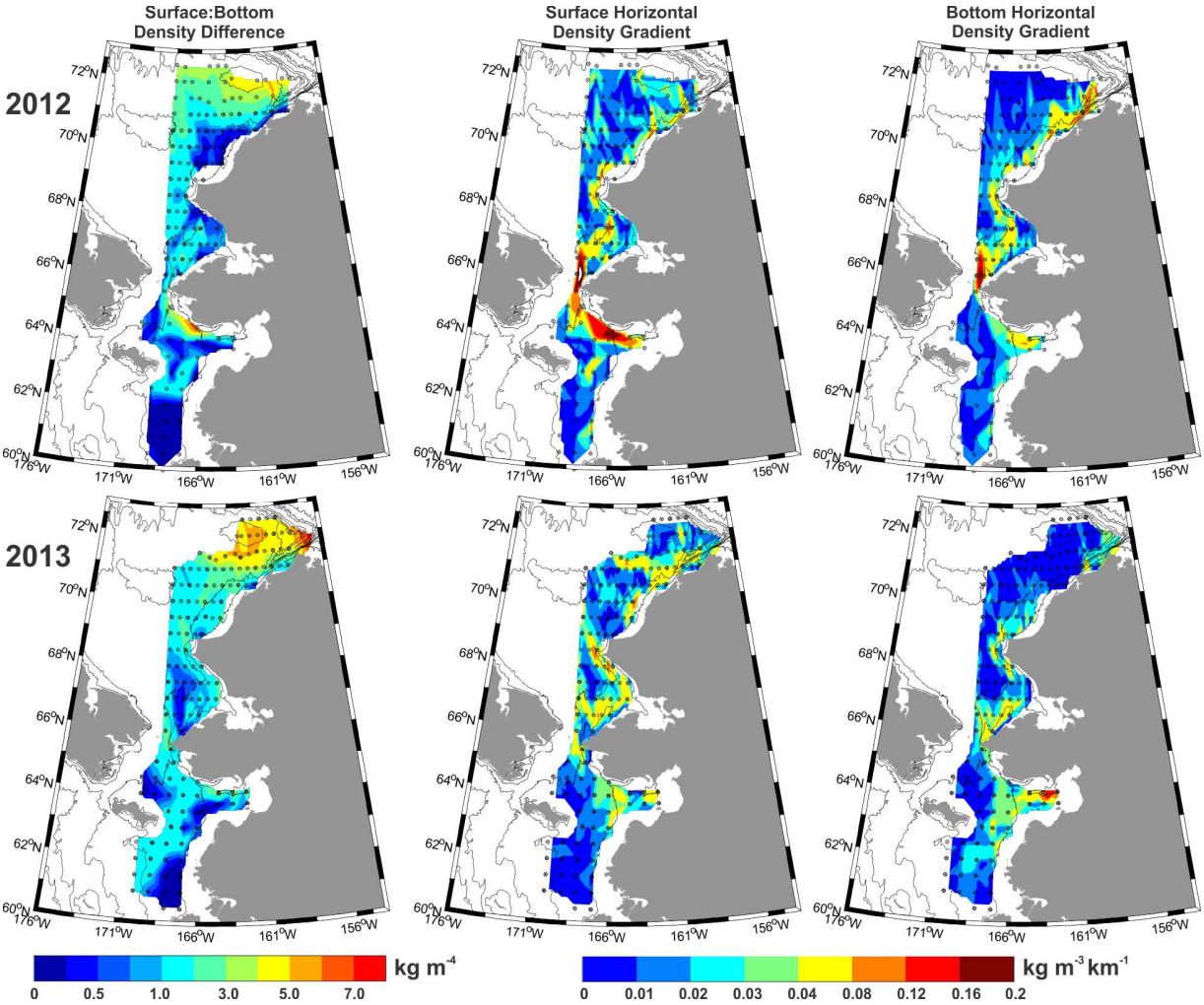

Figure 10. Stratification and fronts in 2012 (top) and 2013 (bottom). Left column shows the difference between the near-surface and near bottom water density. Middle column shows the magnitude of the near-surface horizontal density gradient and the right column shows the magnitude of the near-bottom horizontal density gradient.

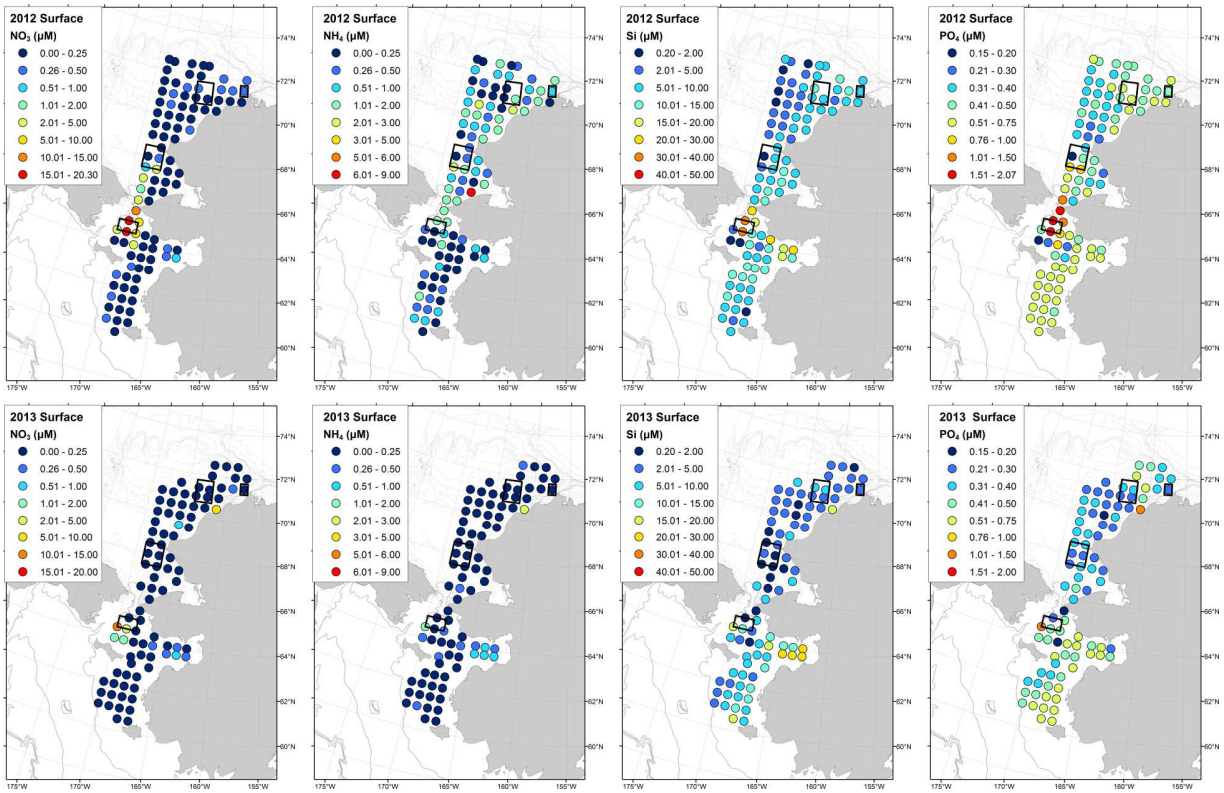

Figure 11. Nutrient concentrations close to the surface (10 m) for 2012 (top row) and 2013 (bottom row). From left to right, the panels show NO_3, NH_4, SiO_4, and PO_4. Black boxes in nitrate plots denote benthic hotspot regions DBO-2 in Chirikov Basin and DBO-3 offshore of Point Hope, DB4 near Hanna Shoal, and DB5 at Barrow Canyon.

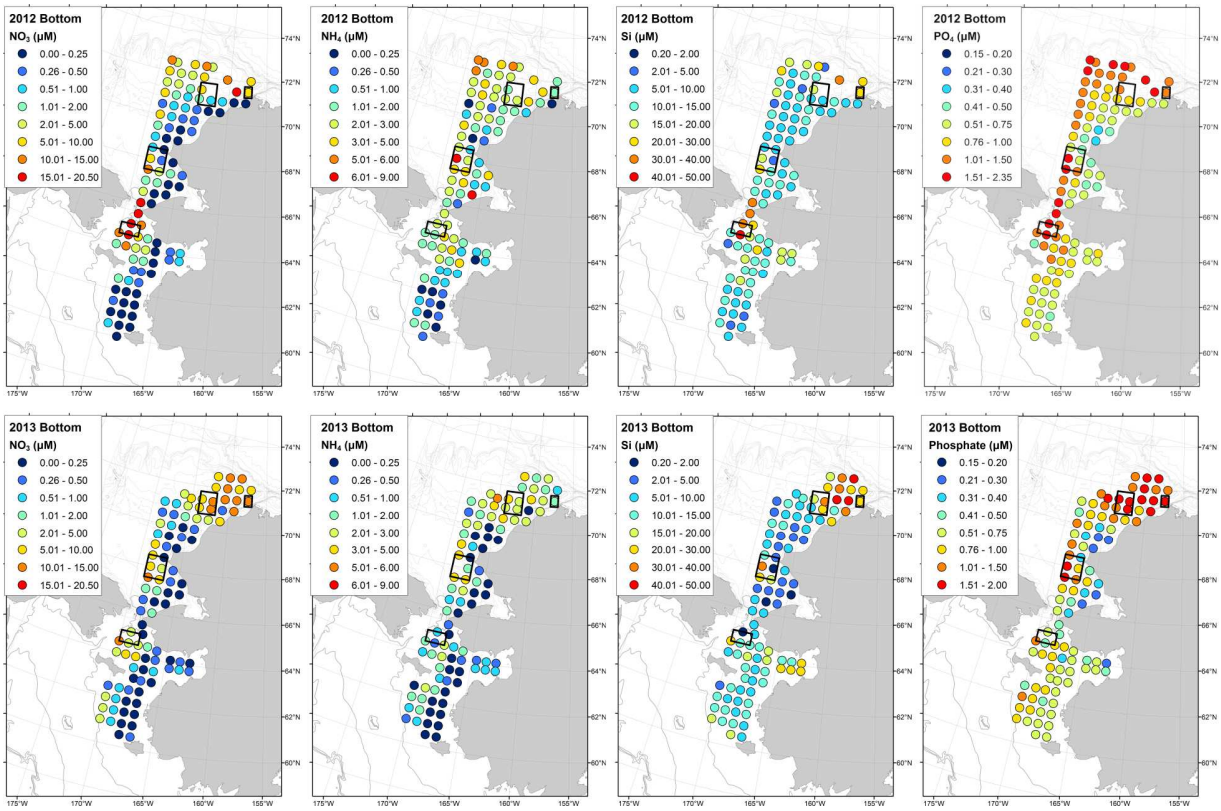

Figure 12. As in Figure 11, but for nutrients close to the seafloor.

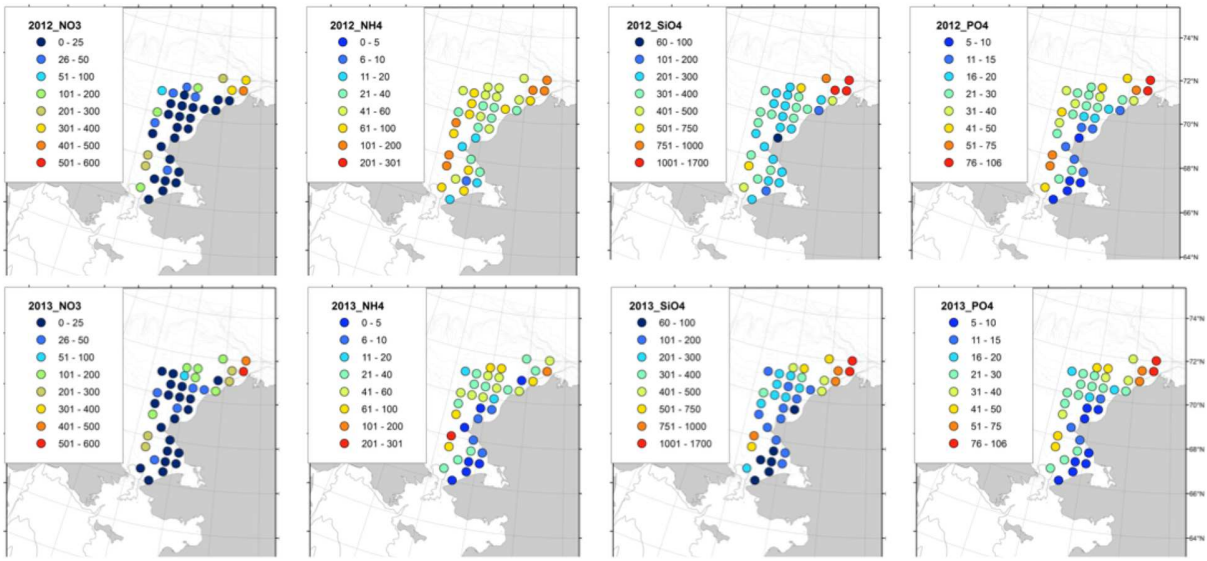

Figure 13. Nutrients integrated through the water column for Chukchi Sea only at stations sampled in both 2012 (top row) and 2013 (bottom row). From left to right, the panels show NO_3, NH_4, SiO_4, and PO_4.

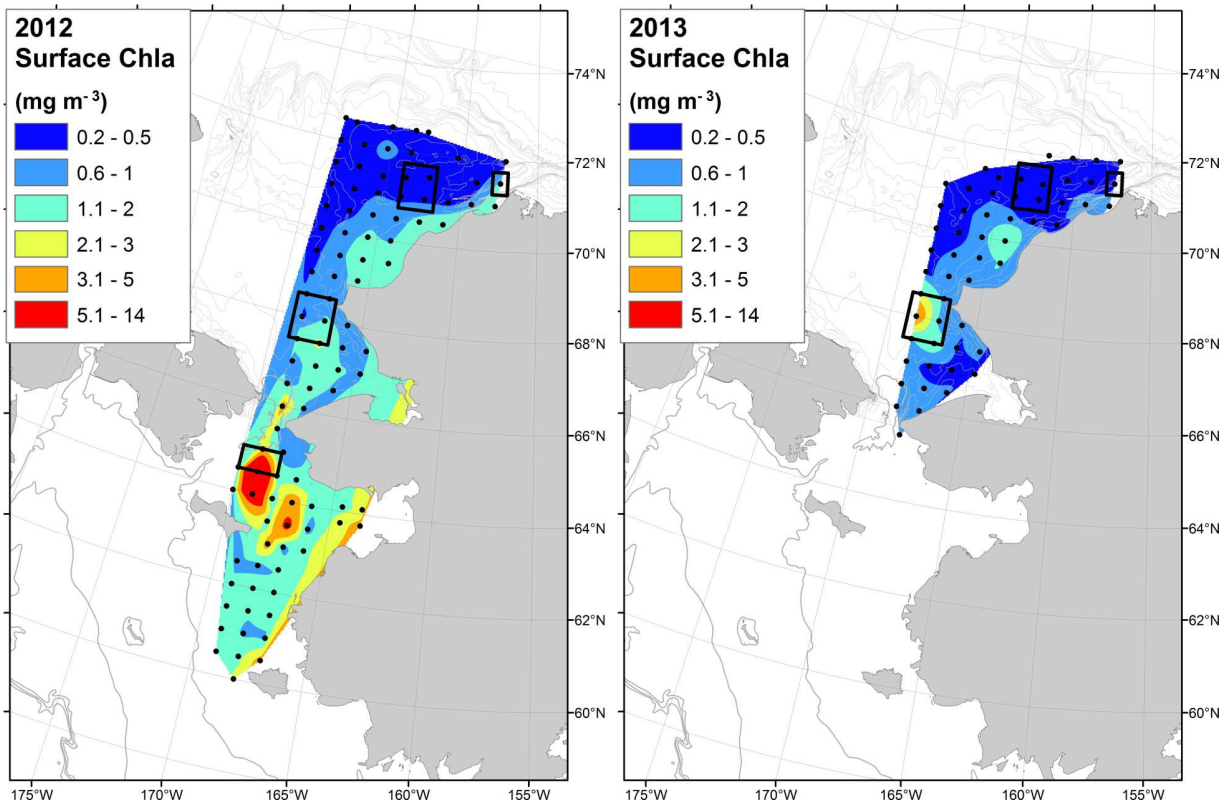

Figure 14. Surface chlorophyll a (mg m^{-3}) from discrete samples for 2012 (left) and 2013 (right). Black boxes denote benthic hotspot regions DBO-2 in Chirikov Basin and DBO-3 offshore of Point Hope, DB4 near Hanna Shoal, and DB5 at Barrow Canyon.

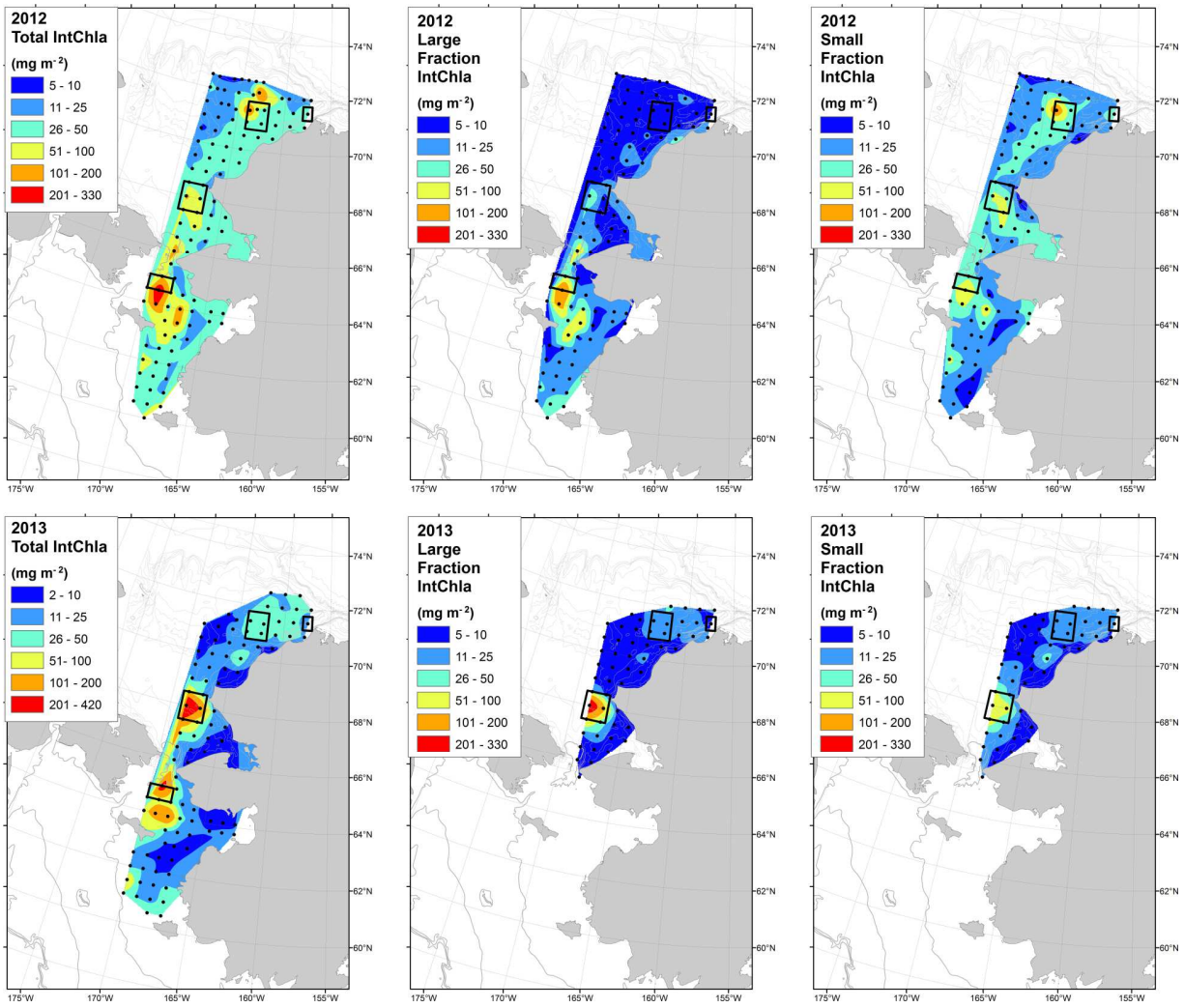

Figure 15. Total, large fraction (> 10 µm) and small fraction (<10 µm) water column integrated chlorophyll a (mg Chl*a* m^{-2}) for 2012 (top) and 2013 (bottom). No size fraction data exist south of Bering Strait in 2013. Black boxes denote benthic hotspot regions DBO-2 in Chirikov Basin, DBO-3 offshore of Point Hope, DBO-4 near Hanna Shoal, and DB5 at Barrow Canyon.